

**A STUDY OF POROUS MEDIA RESISTANCE COEFFICIENTS FOR BRUSH  
SEALS**

by  
**ERDEM GÖRGÜN**

**Submitted to the Graduate School of Engineering and Natural Sciences  
in partial fulfillment of  
the requirements for the degree of  
Master of Science**

**SABANCI UNIVERSITY**

**August 2014**

**A STUDY OF BRUSH SEAL POROUS MEDIA RESISTANCE COEFFICIENTS**

APPROVED BY:

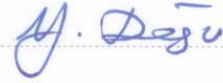
Assoc. Prof. Mahmut F. AKŞİT (*Thesis Advisor*)



Assoc. Prof. Ali KOŞAR



Prof. Dr. Yahya DOĞU



DATE OF APPROVAL: 06/08/2014

© Erdem Görgün 2014  
All Rights Reserved

# **A STUDY OF POROUS MEDIA RESISTANCE COEFFICIENTS FOR BRUSH SEALS**

Erdem Görgün

Mechatronics, MSc. Dissertation, 2014

Thesis Advisor: Assoc. Prof. Mahmut F. AKŞİT

Keywords: Brush Seal, Brush Seal Leakage Performance, Brush Seal CFD Analysis, Porous Media Approach, Porous Media Resistance Coefficients

## **ABSTRACT**

Developments in turbine technologies lead to higher operating temperature and pressure conditions. Parasitic leakage flows around the turbine account for considerable efficiency losses that increase fuel cost dramatically. Brush seal has recently emerged as an improved sealing technology to provide better leakage performance and to replace classical labyrinth seals. In order to optimize efficiency, comprehensive study of the factors causing the leakage is required. The leakage performance of the brush seal is directly related with geometry, operating inlet and outlet boundary conditions, bristle pack configuration. Brush seal flow and pressure profiles with turbine operating conditions become complicated, and analytical formulations remain inadequate to correlate design parameters and leakage performance in operating conditions. Recently brush seals have found ever increasing applications in steam turbines. Literature review indicates that there is very limited studies of brush seal for steam environment. There is also no correlation available for brush seal porosity coefficients in the literature. In an attempt to meet this need, six brush seals have been tested in a rotary test rig up to 100 psi upstream pressure. Analytical correlations and CFD (Computational Fluid Dynamics) simulations have

been performed for test seals and results have been correlated with the test data. Axisymmetric CFD models have been designed to reach anisotropic resistance coefficients for the brush seals based on experiments. Porous Medium Approach has been applied for representing bristle pack. Leakage rate of brush seals (steam environment) has been optimized through CFD models. Moreover, velocity and pressure characteristics in the bristle pack have been illustrated for an optimum solutions. Consequently, empirical correlations for brush seal porosity coefficients have been correlated through a systematic methodology.

# FIRÇA KEÇELERDE GÖZENEKLİ ORTAM AKIŞ DİRENCİ KATSAYILARININ KALİBRASYONU

Erdem Görgün

ME, Yüksek Lisans Tezi, 2014

Tez Danışmanı: Doç. Dr. Mahmut F. AKŞİT

Anahtar kelimeler: Fırça Keçe, Fırça Keçe Sızdırmazlık Performansı, Fırça Keçe HAD Analizi, Gözenekli Ortam Yaklaşımı, Gözenekli Ortam Akış Direnci Katsayıları

## ÖZET

Türbin teknolojilerindeki gelişmeler çalışma koşullarının daha yüksek basınç ve sıcaklıkta gerçekleşmesini sağlamaktadır. Türbin bölgesindeki parazitik kaçak akış önemli ölçüde verimi azaltıp, yakıt masraflarını arttırmaktadır. Fırça keçeler kaçak akış miktarını azaltma konusunda labirent tipi keçelerden daha iyi performans sağlayan bir teknoloji olarak ortaya çıkarılmıştır. Verimliliğin en üst seviyede tutulabilmesi için, kaçak akışı etkileyen faktörleri inceleyen geniş kapsamlı bir çalışmaya ihtiyaç duyulmaktadır. Fırça keçelerin kaçak akış performansı keçe geometrisi, giriş ve çıkış çalışma koşulları, keçelerin konfigürasyonu ile ilişkilendirilmektedir. Fırça keçelerin türbin çalışma koşullarındaki akış ve basınç profilleri değişkenlik göstermekte olup, tasarım parametreleri ile kaçak akış performansı arasındaki ilişkiyi açıklamakta analitik formülasyonlar yetersiz kalmaktadır. Günümüzde fırça keçelerin buhar türbinlerinde kullanımı yaygınlaşmıştır. Yapılan literatür araştırması ile buhar ortamındaki türbin koşullarında yapılan çalışmaların sınırlı sayıda çalışma olduğu görülmüştür. Bununla birlikte, literatürde fırça keçelerin gözenekli ortam akış direnci katsayılarının korelasyonu ile ilgili herhangi bulunmamaktadır. Bu eksikliği gidermek için, altı adet fırça keçe giriş basınç değeri en fazla 100 psi olacak şekilde test edilmiştir. Test edilen keçeler için analitik çalışmalar ve HAD(Hesaplamalı Akışkanlar Dinamiği) analizleri

yapılmış ve sonuçlar test verileriyle ilişkilendirilmiştir. Test verileri ile aksi-simetrik HAD analizleri korelasyonu sonucunda çeşitli basınç farkı seviyelerinde anizotropik akışa dayanım katsayılarına ulaşılmıştır. Fırça keçelerin modellenmesinde gözenekli ortam yaklaşımı kullanılmıştır. Buhar ortamındaki fırça keçelerin kaçak akış miktarı HAD analizleri vasıtası ile optimize edilmiştir. Ayrıca bu çalışmada, elde edilen optimum sonuçlar için basınç ve hız profili ortaya çıkarılmıştır. Sonuç olarak, deneysel korelasyonlar fırça keçelerin gözenekli ortam akış direnci katsayıları korelasyonu için kullanılmıştır.

## ACKNOWLEDGEMENTS

I want express my special thanks to my advisor Mahmut F. Akşit for his support, advice and guidance for my thesis study.

I would also like to thank my committee members Yahya Dođu for his support in computational fluid dynamics, Ali Koşar for his interest in this study and recommendations.

I would like to thank my colleagues Serdar Aksoy, Ertuđrul Tolga Duran, Caner Akcan and Murat Koyuncuođlu for his precious guidance, Ercan Akcan and Abdullah Car for their support and assistance in experimental setup.

I would like to acknowledge that The Scientific & Technological Research Council of Turkey (TÜBİTAK) provides financial support during my MSc. period.

I want to convey my special thanks to each member of Sabanci University Mechatronic Engineering Graduate program. I would like to extend my thanks to Hamza Kazancı, Ali İhsan Tezel, Seyfettin Tolga Yıldırım, Mehmet Emre Kara, Dođan Üzüşen, Taha Çıkım for their amusing friendship and valuable support.

Last but not least, special thanks to most precious thing I own in my life, my family, who make me feel peace of mind. I always feel their support and best wishes.



## TABLE OF CONTENTS

1	INTRODUCTION.....	1
1.1	Brush Seal Structure .....	2
1.2	Main Issues With Brush Seals .....	5
1.2.1	Bristle Stiffening .....	5
1.2.2	Hysteresis .....	6
1.2.3	Blow Down .....	6
1.2.4	Bristle Flutter .....	6
1.3	Problem Statement.....	7
2	BACKGROUND AND LITERATURE REVIEW.....	9
2.1	Historical Review of Brush Seals .....	9
2.2	Leakage Analysis of Brush Seals .....	10
3	MATHEMATICAL MODELLING.....	11
3.1	Calibration of Brush Seal Permeability Coefficients .....	12
3.2	Porosity.....	14
3.3	Porous Media Resistance Coefficients .....	15
3.4	Effective Clearance Calculation .....	17
3.5	Corrected Bristle Height .....	18
4	EXPERIMENTAL SETUP .....	22
4.1	Test Rig.....	23
4.2	Brush Seal Leakage Measurements .....	25
5	CFD ANALYSIS OF LEAKAGE FLOW .....	33
5.1	CFD Model Using Porous Media Approach .....	33
5.2	Boundary Conditions .....	34
5.3	The Mesh .....	36
5.4	Calibration of Resistance Coefficients with Experimental Results.....	38
5.5	Verification of Porous Media Resistance Coefficients with Ideal Gas Approach	39
5.6	CFD Results.....	40
5.6.1	Flow Condition.....	40

5.6.2	Velocity Profile .....	42
5.6.3	Pressure Profile .....	42
6	DESIGN OF EXPERIMENTS .....	47
6.1	Brush Seal Design Variables (The Factors) .....	47
6.2	Main Experiment Design .....	48
6.3	Design of Experiment Results for Ideal Gas Approach .....	50
6.4	Error Calculation for Ideal Gas Approach .....	54
6.5	Design of Experiment Results for Calibration Resistance Coefficient with Pressure Difference .....	55
6.6	Minimum Leakage Solution .....	61
7	CONCLUSION .....	64
8	REFERENCES .....	67
	Appendix .....	71

## LIST OF FIGURES

Figure 1.1: Schematic diagrams illustrating a selection of labyrinth seals. Axial applications: a) straight-through b) stepped c) staggered. Radial applications: d) straight-through e) stepped f) staggered. [3].....	2
Figure 1.2: Brush Seal Structure [5] .....	4
Figure 1.3: Leakage flow in brush seals [5].....	4
Figure 1.4: Bristle Stiffening and Frictional Forces[5].....	5
Figure 3.1: Selected points in fence-upstream and fence-downstream surfaces .....	16
Figure 3.2: Bristle diameters for unwrapped geometry .....	19
Figure 3.3: Corrected bristle height and length calculations .....	20
Figure 3.4: Corrected bristle height change.....	21
Figure 4.1: Schematic and connections of the test rig .....	22
Figure 4.2: Trimetric view of seal housing assembly .....	23
Figure 4.3: Isometric view of rotor holder assembly.....	24
Figure 4.4: Leakage flow rate of Seal #1 for three different cycles .....	25
Figure 4.5: Effective Clearance of Seal #1 average of three different cycles .....	26
Figure 4.6: Leakage flow rate of Seal #2 for three different cycles .....	26
Figure 4.7: Effective Clearance of Seal #2 average of three different cycles .....	27
Figure 4.8: Leakage flow rate of Seal #3 for three different cycles .....	27
Figure 4.9: Effective Clearance of Seal #3 average of three different cycles .....	28
Figure 4.10: Leakage flow rate of Seal #4 for three different cycles .....	28
Figure 4.11: Effective Clearance of Seal #4 average of three different cycles.....	29
Figure 4.12: Leakage flow rate of Seal #5 for three different cycles .....	29
Figure 4.13: Effective Clearance of Seal #5 average of three different cycles.....	30
Figure 4.14: Leakage flow rate of Seal #6 for three different cycles .....	30
Figure 4.15: Effective Clearance of Seal #6 average of three different cycles.....	31
Figure 4.16: Variation of leakage flow rate for Seal #1&6 .....	31
Figure 4.17: Variation of effective clearance for Seal #1&6.....	32
Figure 5.1: Typical brush seal geometry .....	33
Figure 5.2: Brush Seal Design #1 CFD Model a) Dimensions are inches b) Dimensions are millimeters .....	35

Figure 5.3: Typical brush seal mesh for CFD analysis.....	37
Figure 5.4: Velocity vectors for optimal solution at turbine operating condition a) Including downstream and upstream region b) Only fence and pack region .....	41
Figure 5.5: Velocity streamlines for optimal solution at turbine operating condition....	42
Figure 5.6: Absolute pressure distribution for optimal solution in [bar] at turbine conditions.....	43
Figure 5.7: Axial pressure distribution between front and backing plate for optimal solution at turbine operating conditions.....	44
Figure 5.8: Radial pressure distribution on front and backing plate surface for optimal solution at turbine operating conditions.....	45
Figure 5.9: Axial pressure distribution on rotor lower surface for optimal solution at turbine operating conditions .....	46
Figure 5.10: Axial pressure distribution on rotor upper surface for optimal solution at turbine operating conditions .....	46
Figure 6.1: Main effect plots of factors for Ideal Gas Approach (in SI units).....	53
Figure 6.2: T-v Diagram for water and steam [37].....	55
Figure 6.3: Streamwise Resistance Coefficients ( $\Delta P = 1.05, 3.44$ and $5.5$ bar) for porous regions, line-to-line clearance configuration .....	56
Figure 6.4: Transverse Resistance Coefficients ( $\Delta P = 1.05, 3.44$ and $5.5$ bar) for porous regions, line-to-line clearance configuration .....	56
Figure 6.5: Main effect plots of factors for Pressure Difference Approach .....	59
Figure 6.6: Pareto Chart for leakage rate .....	60

## LIST OF TABLES

Table 1.1: Haynes 25 – 10% cold worked, material properties at room temperature [4].	3
Table 5.1: CFD analysis cases and related model parameters .....	38
Table 5.2: Calibrated resistance coefficients .....	39
Table 5.3: Calibration of averaged mass flow rate and effective clearance between test results and CFD .....	39
Table 5.4: Comparison of Resistance Coefficients for Calibrated CFD Results with Tests and Analytical Estimation.....	40
Table 6.1: Level values of factors.....	49
Table 6.2: Reference and DOE conditions for calculation resistance coefficients.....	50
Table 6.3: Geometric Specifications for Design of Experiments for Ideal Gas Approach .....	51
Table 6.4: Design of Experiments Results for Ideal Gas Approach.....	52
Table 6.5: Design of Experiments Results for Calibration Resistance Coefficients with Pressure Difference.....	57
Table 6.6: Fit Values for Coefficients of Leakage Rate for both Coded and Actual Values .....	61
Table 6.7: Response and Algorithm Settings.....	62
Table 6.8: Optimal Solution for Calibration Resistance Coefficients with Ideal Gas and Pressure Difference Approach .....	63

## NOMENCLATURE

$2a$	=	Major axis
$2b$	=	Minor axis
$Clr_{eff}$	=	Effective Clearance
$d$	=	Bristle diameter
$g$	=	Gap
$g_c$	=	Gravitational constant for British units
$K$	=	Permeability
$\dot{m}$	=	Mass flow rate
$P_u$	=	Upstream pressure
$P_d$	=	Downstream pressure
$\Delta P$	=	Pressure load
$R$	=	Brush seal inner radius
$R_c$	=	Specific Gas Constant
$R_{pinch}$	=	Seal radius at pinch point
$t$	=	Brush seal thickness
$u$	=	Velocity
$x$	=	x-coordinate
$y$	=	y-coordinate
$z$	=	z-coordinate

### **Greek Symbols**

$\alpha$	=	Effective inertial quadratic resistance
$\beta$	=	Effective linear viscous resistance
$\gamma$	=	Specific ratio of heats
$\varepsilon$	=	Porosity
$\theta$	=	Cant angle
$\mu$	=	Dynamic viscosity
$\rho$	=	Density

### **Abbreviations**

$BDE$	=	Bristle Density
$BDIA$	=	Bristle Diameter
$BH$	=	Free Bristle Height
$BH_{cor}$	=	Corrected Free Bristle Height
$BPT$	=	Bristle Plate Thickness
$CA$	=	Cant Angle
$CFD$	=	Computational Fluid Dynamics
$FBH$	=	Free Bristle Height
$FF$	=	Flow Function

FH = Fence Height  
FPT = Front Plate Thickness  
NR = Number of Rows

# 1 INTRODUCTION

Seal technology has a key role in gas turbines for cooling and leakage flows, Modern turbines require higher efficiency which is provided by higher pressure ratios, new manufacturing methods, new cooling systems. Advances in sealing technology have considerably impact on decreasing operational costs and fuel consumption. Leakage performance is one of the major concerns of turbo-machinery applications which has significant effect on overall performance. Seals decrease leakage rate in turbine and compressor applications, and they are also have impact for controlling rotor dynamic stability in transient conditions. Labyrinth seals are inadequate in terms of leakage performance for most applications in turbines. Brush seal is an answer to reduce leakage rate and increase turbine performance as an alternative for labyrinth seals.

Previous studies reveal that approximately one-third of the total stage efficiency is lost due to leakage rate in clearance region [1,2]. Therefore, decreasing mass flow rate between rotor and stator parts is most important objective for turbo-machinery performance studies. For this reason, design of seals is one of the biggest issues on system performance. The most influential parameter is clearance level between rotor and stator for identifying leakage performance whereas excessive levels of clearance may lead to instabilities and decrease overall efficiency. Brush seal is a new sealing technology to decrease loss of efficiency. Its performance is correlated with effective clearance levels.

Laby seal is a sealing element which has been applied since gas and steam turbines are invented. It uses flow throttling through knife edges that can be configured in many ways. Design parameters of labyrinth seals can be expressed as number of tooth, clearance, throttle and dimensions in geometry. Although, labyrinth seal technology has been developed over decades, mass flow rate in clearance regions is excessive making it inadequate to meet necessary performance criteria for recent competitive turbine technology. Therefore, a next generation of seals have been developed combining abrasible materials with laby sealing applications. Applications of abrasible materials



leads to reduce clearances and with optimized geometries, while they cause erosion and wear of the blades. Unlike rigid laby seals, flexibility of brush seal provides further reduction of effective clearance and flow rate and damp forces that result from oscillations on rotor. Brush seal is a new innovative technology, and it is preferred over laby seal in critical regions of turbo-machinery due to its superior leakage performance.

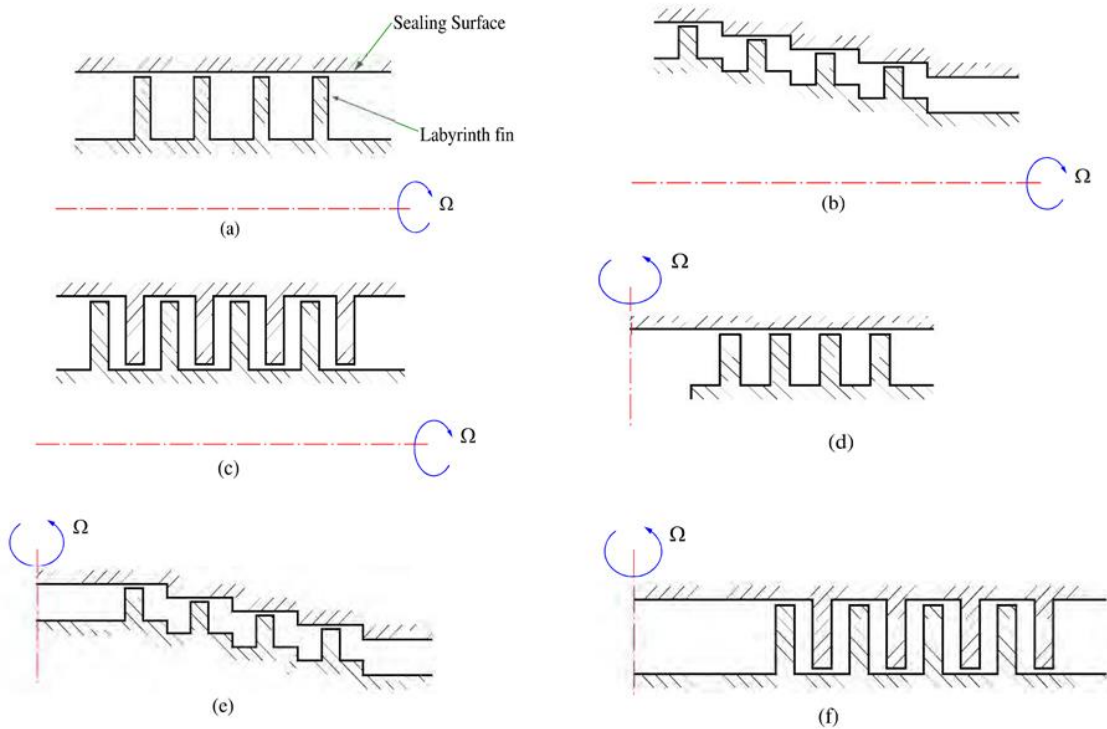


**Figure 1.1: Schematic diagrams illustrating a selection of labyrinth seals. Axial applications: a) straight-through b) stepped c) staggered. Radial applications: d) straight-through e) stepped f) staggered. [3]**

## 1.1 Brush Seal Structure

The brush seal is composed of a pack of fine diameter which is compressed between front plate and backing plate. It is made of Haynes 25 fibers that have diameter between 0.05 and 0.15 mm. Fiber density ranges 1500 to 2500 fibers per inch of seal circumferences. Haynes 25 is a cobalt based super alloy which has perfect resistance for high temperature, oxidation and deformation. It is shaped and manufactured by traditional methods. Main properties of Haynes 25 are revealed in Table 1.1

<b>Haynes 25 – 10% cold worked, Material Properties [52]</b>	
Nominal chemical composition, weight percent	Co(51%)–Ni(10%)–Cr(20%)–W(15%)–Fe(3%)–Mn(1.5%)–Si(0.4%)–C(0.1%)
Tensile yield strength at room temperature	725MPa
Ultimate tensile strength at room temperature	1070MPa
Modulus of elasticity at room temperature	225,000MPa
Density at room temperature	9.13g/cm <sup>3</sup>
Poisson's ratio	0.3

**Table 1.1: Haynes 25 – 10% cold worked, material properties at room temperature [4]**

The brush seal is mounted between rotor and stator. Figure 1.2 illustrates brush seal structure and design parameters [5]. BH refers to free bristle height, FH shows fence height, and rotor radius is denoted by R. Brush seal is placed between low pressure and high pressure regions around rotating shafts. Fluid moves in axial direction from upstream region which has higher pressure to downstream region which has lower pressure. Front plate clamps and holds bristles in place while backing plate is used for mechanical reinforcement under pressure load. Brush seal is fixed at stator typically with small interference on rotor surface. While seal is located in a static member, bristles contact with rotor at an acute angle. This angle is between rotor surface normal and bristle direction is called cant angle or lay angle. Cant angle allows bristles to bend and deform when interference occurs during rotor excursions, which significantly reduces contact severity. Cant angle is designed mostly between 35° and 55°. Since brush seal is applied to reduce leakage, mass flow rate that move through brush seal becomes major parameter to determine performance of the design. Fence height is the radial distance between backing plate inner radius and rotor surface, and free bristle height is defined as radial distance between pinch point and seal inner radius.

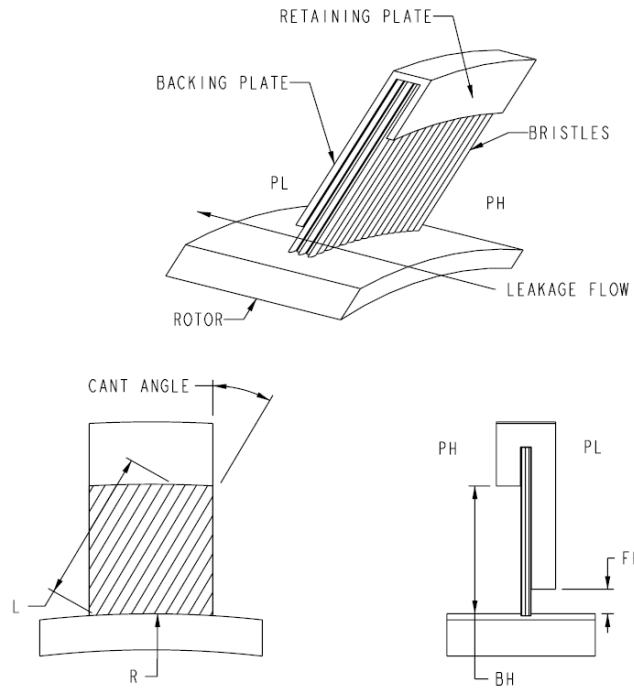


**Figure 1.2: Brush Seal Structure [5]**

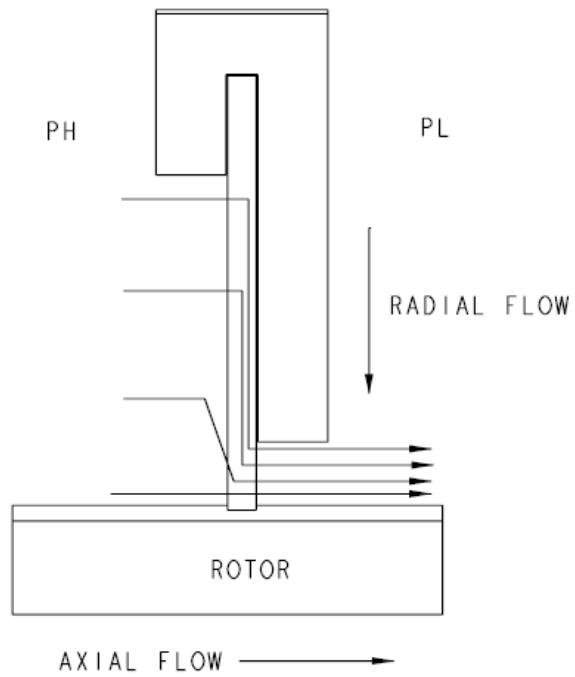


**Figure 1.3: Leakage flow in brush seals [5]**

## 1.2 Main Issues With Brush Seals

The interaction between pressure difference and flexible seal structure results in some critical brush seal behavior such as bristle stiffening, hysteresis, blow-down and bristle flutter. Under operating conditions, leakage performance of the brush seal is usually influenced by these phenomena.

### 1.2.1 Bristle Stiffening

Bristles are forced to move toward backing plate direction that Figure 1.4 illustrates causing bristle stiffening behavior under applied pressure load. Under pressure bristles stick to each other and last column sticks to vertical surface of the backing plate. As a result of high frictional resistance with pressure load, stiffness of seal increases. Therefore, rotor excursions result in high wear rates which have adverse impact on leakage performance and service life.

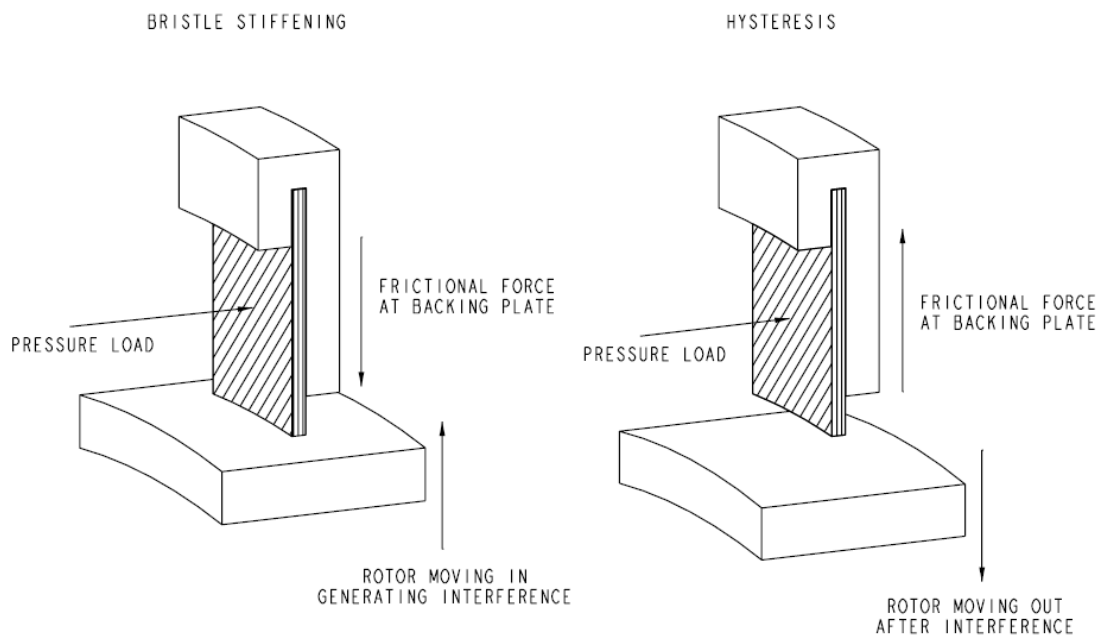


Figure 1.4: Bristle Stiffening and Frictional Forces[5]

### **1.2.2 Hysteresis**

Bristles are forced towards outer direction when rotor excursions are occurred during transient conditions. Rotor excursion due to eccentricity or thermal growth applies force and displacement to bristles before turbine reaches steady state conditions. If seal is not designed properly, when rotor returns to initial position in steady state, bristles cannot return to their original radial positions due to bristles sticking at the backing plate. Hysteresis is important phenomenon which has impact on leakage performance. Hysteresis also explains that leakage rate is changing between pressure cycles. In other words, mass flow rate may be measured differently for same pressure levels since hysteresis alters bristle-rotor clearance after pressure difference is applied.

### **1.2.3 Blow Down**

‘Blow-down’ is defined as the bristles close to the upstream region move radially towards rotor. Total axial pressure is decreasing from high pressure region to low pressure region in bristle pack. Therefore, bristles near downstream region encounter large axial pressure load whereas upstream side bristles have a tendency to move in the rotor direction. There are two main factors which have influence on blow-down; axial pressure due to pressure difference and aerodynamic forces under bristle tips. Increasing the height of the backing plate may be beneficial to reduce the effect of blow-down in downstream side bristles, while high lay angle and pressure difference rise the effect of blow down.

### **1.2.4 Bristle Flutter**

Upstream side of bristles have tendency for vibration, they act under relatively low pressure load. High turbulence level or jet flow results in oscillations on pressure level over these bristles. Flutter is mostly coincided with air brush seals. Wear rate of upstream side bristles can be higher than downstream side which causes non-uniform wear rate in axial direction. One should select bristle density and backing plate geometry carefully to prevent bristle flutter.

### 1.3 Problem Statement

The efficiency of the brush seal is directly related to its leakage rate. One should design seal to maintain minimum leakage during entire operating time. Ferguson [6] stated that a brush seal can reduce leakage rate to down to approximately %10 of the best possible finned labyrinth seal which has a clearance of 0.7 mm (0.027 in). Therefore, improve leakage performance, improving and optimizing brush seal design further analyses are needed.

The leakage performance of the brush seal is directly related to geometry, operating inlet and outlet boundary conditions, bristle pack material. Brush seal leakage rate under turbine operating conditions becomes so complicated simple application of analytical equations are inadequate to achieve desired results. In spite of the fact that brush seals have been utilized in many turbine applications, these seals are preliminary designed by experimental work. Details of the seal designs are not fully analytically studied. The available equations from literature cannot provide sufficient details for correlation between design and brush seal performance under operating conditions. Literature review brings out that there is a need for more study in especially for flow analyses of brush seals for steam environment.

Brush seal leakage characterization have been performed by using correlated CFD models. Flow analyses have been conducted with various design parameters and resistance coefficients. In order to estimate the values of flow resistance coefficients, various methods have been developed. Mathematical models, experimental results, analysis models are presented in this study. Unlike other studies in literature; once resistance coefficients are calibrated, analyses are also performed for steam environment.

Among different approaches to model brush seal leakage flow, porous medium modeling of brush pack provides the most insight to help designers. However, flow resistance/porosity coefficients for these porous media CFD models have to be calibrated with experimental seal leakage test data for each design. In this work, a design of experiments test matrix has been defined with some typical ranges of main seal design parameters. The selected design space has been uniformly sampled using orthogonal arrays. The results have been evaluated to determine strong and weak factors affecting flow resistivity. Polynomial fits and empirical relations have been derived using the

design factors that strongly affect brush flow resistivity. It is expected that these empirical relations may guide designers when they estimate performance of different brush seal designs. The objective of this study are estimating resistance coefficients for conditions which cannot supported by test results. Models in air and steam environment are aimed to calibrate with resistance coefficients. The contribution of this study is allowing estimation of resistance coefficients for different fluid environments.

## 2 BACKGROUND AND LITERATURE REVIEW

In the evolution of the gas and steam turbines, sealing technology is one of the most important issues in order to increase performance of the whole system. Therefore, various types of seals are applied in turbine and compressor systems. Labyrinth seal is the first technology that have been used for turbines. Clearance of laby seals increase with wear which leads to loss of efficiency. Moreover, identifying optimum sealing solution under harsh operating conditions is a challenge.

### 2.1 Historical Review of Brush Seals

The invention of brush for sealing purposes is mentioned in a patent at the beginning of the 20<sup>th</sup> Century. However, it is not integrated in any turbine until metal brush seal is applied in GE J-47 engine tests [7].

Brush seal has been re-applied in aviation technologies in 1980s [8,9]. Rolls Royce integrated brush seal technology in IAE V2500 engine to increase overall performance. Gorelov et al. [10] and Ferguson [6] stated that brush seal improve leakage performance of the gas turbines compared to labyrinth seals. Brush seal were firstly applied in an industrial gas turbines in the 1990s [11, 12]. Holle et. al. [13] stated that U.S. Army integrated brush seals into gas turbines with Teledyne CAE [14]. Superiority of brush seal over labyrinth seal has been successfully demonstrated with acceptable rate of rotor interference which is compensated by brush seal [13].

The application of the brush seal has been dramatically increased during last twenty years whereas detailed study over leakage performance in various conditions is still a requirement to determine important performance parameters. Owen et al calculated heat generation dissipation over bristle pack with conduction inbetween bristles [15]. Another study reveals a computational model for fluid in order to observe change of structural properties [16]. Demiroglu illustrated temperature distribution around rotor surface and bristle pack domain with infrared thermograph method [17]. Analytical and numerical study over temperature and leakage flow has been conducted by Dogu et al. with a two-dimensional axisymmetric CFD model [18].



## 2.2 Leakage Analysis of Brush Seals

It is challenging to successfully analyze fluid dynamics of large number of bending bristles under operating conditions. The obstacles that are encountered during leakage analysis of brush seals can be listed as compliance, hysteresis, blow-down, 3-D flow, rotor interference, wear, hydrodynamic lift and bristle flutter [5]. The effect of compliance can not be easily defined as each bristle acts individually and distance between bristles may change with operating conditions. Hysteresis also results in change of seal clearance due to frictional interlocking. Blow-down leads to change of bristle density under pressure load. Since fluid moves in axial, radial and tangential directions, the analysis should be performed in 3-D or axisymmetric model. NASA researchers developed representation of fluid movement system to watch mass flow profile over brush seal [19, 20]. Various flow characteristics such as rivering, jetting, vortices are observed in leakage flow through brush seals [21]. Carlile et al. [22] stated that bristles open for a path at some locations which results in gaps between bristles for excess fluid flow.

Time dependent pressure profiles are determined firstly by using pressure probes in the upstream and downstream regions. Braun illustrated that pressure is decreasing linearly from upstream to downstream across the bristle pack [23]. Braun and Kudriatsev developed a simulation for fluid flow based on 2-D time dependent Navier-Stokes equations [24, 25]. Another study correlated laminar flow over bristles which are modeled as circles [26]. The influence of the bristle gap and rotor triggered swirl of mass flow rate between rotating and stationary parts are investigated with staggered 2-D bristle pack model [27]. Applying a finite difference method, analytical model of bulk flow approach is constructed by Hendricks [28, 29] and Braun [30]. Another approach is treating brush seal as a 2-D axisymmetric Darcian anisotropic porous media medium [31]. Computational fluid dynamics model with porous medium approach is used to estimate leakage rate, pressure distribution, velocity streamlines and kinetic energy for brush seal [32, 33]. Turner illustrated mass flow profile and velocity field for the case where clearance exists between bristle pack and rotating surface [34].

### 3 MATHEMATICAL MODELING

The structural and leakage performance of the brush seal is determined primarily by the behavior of bristles when pressure load is applied. Before any turbine or engine application brush seal structural stability and leakage performance should be studied. The steady state clearance, which is the distance between rotor surface and bristles, have crucially influence on the performance of the seal. This section covers analytical study related to seal leakage and flow evaluation.

The velocity and pressure characteristics of fluid in the vicinity of the brush seal and within the bristle pack have impact on the seal durability and leakage performance. The motion of the bristles during operation is a function of force balance between elastic, aerodynamic and frictional forces among bristles and the backing plate. Due to its simplicity and compactness, the porous medium approach is applied to the brush pack in order to determine flow characteristic and sealing performance. Various flow models have been studied to model brush seal system. In the first model, voids within bristles are modeled as fluid. This method has obstacles to simulate the flow behavior since randomly distributed bristles are moving, bending, flexing, twisting, squeezing under turbine operating conditions. Second approach offers semi-empirical bulk flow methods which are based on flow-driven non-dimensional parameters and geometrical configurations. Bulk flow methods can be correlated with experimental data, however, they fall short to illustrate mass flow rate and pressure distribution with respect to seal geometry parameters, initial and boundary conditions in steady state conditions. Another approach is developed by treating the entire bristle pack as a single porous medium with identified flow/leakage resistance parameters. The porous medium approach relies on applying the Navier–Stokes equation with different flow resistance parameters in different flow directions. Resistance coefficients correlated with friction between flow and bristles. For the highly resistive porous media, this equation is simplified by neglecting the inertial terms which yields a balance equation between pressure gradient and flow resistance terms. Porous media approach has been applied to brush seals in order to identify flow-driven properties such as leakage rate, pressure, velocity, temperature and kinetic energy.

The porous medium approach may differ from the first two methods by providing the pressure distribution inside of bristle pack in addition to leakage and axial pressure estimations. The velocity field in the close vicinity of bristle pack can be also observed in the light of porous medium approach. Due to its superiority porous media approach has been used in this study.

In order to match the experimental data, it has been concluded that bristle pack is well represented by two distinct regions of resistance coefficients. These regions are the fence height (rotor-backing plate radial distance) region and the pack region (along the backing plate) that have different structural and flow behavior during operation.

### 3.1 Calibration of Brush Seal Permeability Coefficients

During the modeling of the presented porous media model the leakage flow is assumed to be turbulent and compressible. The reduced Navier–Stokes equations governing the fluid flow in the upstream and downstream velocity profile can be expressed in Cartesian tensor notation as:

$$\frac{\partial \rho u_i}{\partial x_i} = 0 \quad (3.1)$$

$$u_j \frac{\partial \rho u_i}{\partial x_j} = -\frac{\partial P}{\partial x_i} + \mu \frac{\partial^2 u_i}{\partial x_j \partial x_j} \quad (3.2)$$

In addition to Navier-Stokes equation, Darcy porosity model provides the relationship between pressure gradient and viscosity in porous region. It is expressed as below:

$$-\frac{\partial P}{\partial x_i} = \frac{\mu}{K_i} u_i \quad (3.3)$$

$x_i$  refers to orthotropic flow directions,  $K_i$  means permeability of the porous media and  $u_i$  is the superficial velocity in the orthotropic flow direction. Superficial velocity is a hypothetical fluid velocity for calculated mass flow rate by ignoring influence of porous region. In the absence of porosity effect,  $u_i$  is expressed in terms of average velocity ( $u$ ) and porosity ( $\epsilon$ ):

$$u_i = u / \varepsilon \quad (3.4)$$

Porosity model involves only viscous resistance terms in Equation (3.3). Extended version of linear Darcian model is given in Equation (3.5). This is also called non-Darcian porosity model for more precise resistance relationship as:

$$-\frac{dP}{dx_i} = (\alpha_i |u_i| + \beta_i) u_i \quad (3.5)$$

$\alpha$  refers to effective inertial quadratic resistance, and  $\beta$  refers to effective linear viscous resistance.

Directional Loss Model can be applied as the momentum source throughout an anisotropic porous region. The advantage of this method is that it allows directional resistance which is compatible with cant angle of bristle pack. In streamwise direction, the model allows varying resistivity in space. Transverse directions are perpendicular to streamwise direction which can be modeled as a factor of streamwise resistance coefficients.

Porous media approach is described with respect to cant angle, porosity and linear, quadratic, streamwise, transverse resistance coefficients.

In this study, leakage and pressure conditions are calibrated with experiments and CFD results. Matching empirical and computational data provide resistance coefficient values for both streamwise and transverse directions. It is also possible to make definitions in the axial and radial directions or by considering the cant angle of brush seal. Details of permeability coefficient calibration process are given in the following sections.

In a brush seal flow analysis, porous region is separated into two domains which are called fence and pack regions with different permeability coefficients to improve model quality and help the empirical matching procedure. Backing plate holds bristles in place and supports bristle against axial motion in the pack region. Therefore, bristles have %20-25 higher resistance coefficient values compared to fence region [36]. Backing plate also reduce leakage as the pressure profile on backing plate is much higher than the downstream pressure. In the fence height region, bristles deflect axially downstream under pressure load opening interbristle distance and increasing porosity. In summary,

the upper region of the bristle pack has higher values of flow resistance coefficients than fence height region.

### 3.2 Porosity

Porosity is mainly determined by bristle density and geometric configuration of layers which are two fundamental specifications of brush region.

Porosity ' $\varepsilon$ ' is calculated for an ideal configuration of circular cylinders. When their cross sections are considered in tangential direction, elliptical sections are obtained due to bristle cant angles. In Equation (3.6), ' $g$ ' denotes bristle-bristle gap, ' $2a$ ' indicates the major axis, and ' $2b$ ', is the minor axis.

$$\varepsilon = 1 - \frac{\pi}{2\sqrt{3}\left(1+\frac{g}{2a}\right)\left(1+\frac{g}{2b}\right)} \quad (3.6)$$

The bristle-rotor interface, for most brush seals, represents a plane of small curvature. Since rotor and bristles are located in axisymmetric plane, the interaction between bristles and rotor surface can be illustrated as a small bending plane. Fluid flow is observed between bristles and through bristle-shaft clearance.

$$\varepsilon = 1 - \frac{A_s}{A_t} = 1 - \frac{N_t \pi}{4wL \cos(\theta + \varphi)} \quad (3.7)$$

Unpacked porosity is calculated from the number of bristles ' $N_t$ ' is counted for specified area ' $A_t$ ', length ' $L$ ', and width ' $w$ ' revealed in terms of bristle diameters. The area occupied by the bristles ' $A_s$ ' is elliptical and expressed as the ratio of the cylindrical bristle area to  $\cos(\theta + \varphi)$ , where  $(\theta + \varphi)$  represents the interface angle with respect to the bristle. ' $\theta$ ' refers to the angle from bristle attachment, and  $\varphi$  is the angle from the rotor centerline.

If the gap  $g$  is known, Equation (3.6) may be used to calculate porosity. In other condition, Equation (3.7) can be applied by using geometric specifications of bristle pack. Moreover, if the brush thickness,  $t$ , and the number of bristle rows,  $NR$ , are given for an ideal spacing of  $d + \varepsilon_0$ , where  $d$  is bristle diameter,

$$D = 2\varepsilon_0 + d \quad (3.8)$$

Where the number of bristle rows is obtained from the bristle pack density ' $\eta$ ' which is equal to number of bristles per circumferential seal length as

$$NR \approx 1.05\eta D / \cos \theta \quad (3.9)$$

where ' $\theta$ ' is the lay angle and D is the corrected bristle diameter which takes into account the bristles roughness and surface asperities.

Equation (3.6) and (3.8) provides an expression for porosity ( $\varepsilon$ ) in terms of  $\varepsilon_0$  and d,

$$\varepsilon = 1 - \frac{\pi}{2\sqrt{3}\left(1+\frac{\varepsilon_0}{d}\right)^2} \quad (3.10)$$

Brush porosity is strongly three-dimensional, and yet is most often treated as an averaged two-dimensional property. Modeling and analyzing thousands of bristles in three-dimension is almost impossible. Therefore, porosity is considered as an averaged two-dimensional property.

Minimum pack thickness is expressed by using corrected bristle diameter and the total number of bristle rows from Equation (3.9):

$$\langle t \rangle_{min} = (NR - 1) \sqrt{D^2 - \frac{(1.05D)^2}{4}} + D \quad (3.11)$$

The above-mentioned equations provide realistic geometry and boundary conditions for the simulation of the brush seals with porous medium approach.

### 3.3 Porous Media Resistance Coefficients

The full porous model can be reached with both generalization of Navier-Stokes equations and Darcy's law. The model involves advection and diffusion terms, hence it is suitable for closed area flow. An anisotropic version of Darcy's law is obtained in Equation 3.12 as actual velocity component (U) is written in terms of inverse of the resistance tensor and pressure gradient.

$$U = -R^{-1} \nabla P \quad (3.12)$$

where the gradient of pressure is written for single dimension:

$$\frac{dP}{dx} \approx \frac{\Delta P}{\Delta L} \quad (3.13)$$

The relationship between velocity and pressure for selected two points in Figure 3.1, is expressed via Bernoulli Equation. Assuming the potential energy terms for chosen points are equal since there is no change in the downstream and upstream surface of fence region, one can write  $\mu_1 = \mu_2 = \mu$  and:

$$P_1 + \frac{1}{2}\rho_1 V_1^2 = P_2 + \frac{1}{2}\rho_2 V_2^2 \quad (3.14)$$

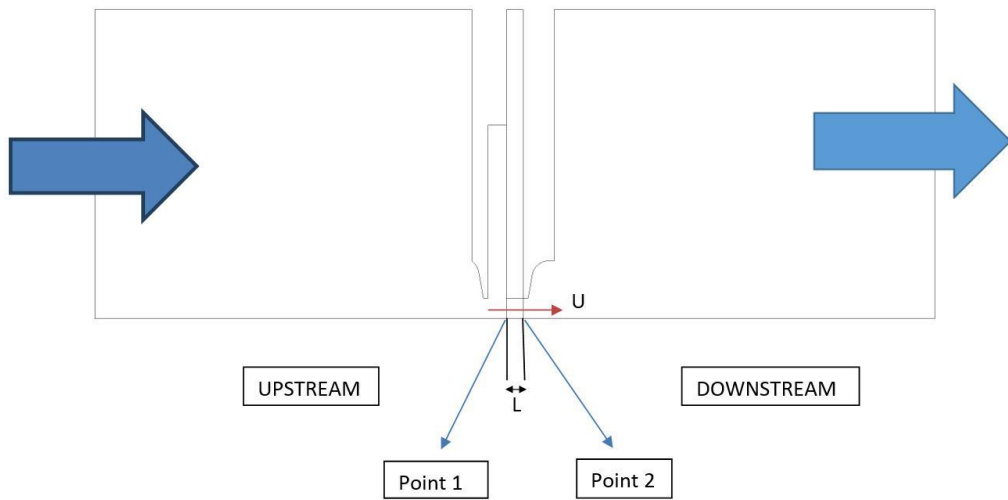


**Figure 3.1: Selected points in fence-upstream and fence-downstream surfaces**

Previous studies reveal that the axial velocity at fence-upstream surface is significantly decreasing and approaching close to zero. As flow encounters bristle pack, which have high flow resistance, fluid diffuses through upper area. A stagnation point occurs at Point 1 where axial velocity can be assumed as zero.

$$P_1 - P_2 = \frac{1}{2}\rho V_2^2 \quad (3.15)$$

As pressure difference illustrated as  $P_1 - P_2 = \Delta P$ , velocity for second point is formulated as:

$$V_2 = \sqrt{\frac{2\Delta P}{\rho}} \quad (3.16)$$

$$\text{Ideal Gas Law} \Rightarrow \rho = \frac{P}{R_c T} \quad (3.17)$$

$V_2$  is proportional to square root of density and pressure difference. Assuming that actual velocity refers to average velocity, Equation (3.12) is modified with ideal gas law and correlation of resistance coefficients between reference and current analysis has been reached. Therefore, validation of CFD results with static air tests are critically important for creating base case. The validation of the equation has been completed with test data.

### 3.4 Effective Clearance Calculation

The one dimensional mass flow equation is given as:

$$\dot{m} = \rho AV \quad (3.18)$$

where  $\dot{m}$  is mass flow rate,  $\rho$  is density,  $V$  is velocity and  $A$  is the area of the flow. The following flow function ( $FF$ ) is defined in terms of total pressure, total temperature, specific heat ratio and specific gas constant:

$$FF = \frac{\dot{m} \sqrt{T_T}}{P_T A_{eff}} \quad (3.19)$$

Then effective clearance of the brush seal is defined as,

$$Clr_{eff} = \frac{\dot{m} \sqrt{T_T}}{\pi DP_T FF} \quad (3.20)$$

The expression of flow function varies according to pressure ratio and ratio of specific heat,

$$\text{If } \frac{P}{P_T} > \left( \frac{2}{\gamma + 1} \right)^{\frac{\gamma}{\gamma - 1}} \Rightarrow FF = \sqrt{\frac{\gamma g_c}{R}} \sqrt{\left( \frac{2}{\gamma - 1} \right) \left[ \left( \frac{P}{P_T} \right)^{\frac{2}{\gamma}} - \left( \frac{P}{P_T} \right)^{\frac{\gamma + 1}{\gamma}} \right]} \rightarrow \text{Unchoked} \quad (3.21)$$



$$\text{If } \frac{P}{P_T} \leq \left( \frac{2}{\gamma + 1} \right)^{\frac{\gamma}{\gamma - 1}} \Rightarrow FF = \sqrt{\frac{\gamma g_c}{R} \sqrt{\left( \frac{2}{\gamma + 1} \right)^{\frac{\gamma + 1}{\gamma - 1}}} \rightarrow \text{Choked} \quad (3.22)$$

where P is downstream static pressure, P<sub>T</sub> is upstream total pressure, R is air gas constant,  $\gamma$  is specific ratio of specific heat values, g<sub>c</sub> is gravitational constant. Effective clearance value provides an important metric to compare brush seal leakage performance for different cases and geometries.

### 3.5 Corrected Bristle Height

Free bristle height calculations are calculated on brush seal packaged geometry. In conservative calculation, the free bristle height is expressed as multiplication of the free bristle length and cosine of the cant angle. Free bristle height is formulated as the difference between pinch point radius and bristle pack inner radius.

$$BH = R_{pinch} - R \quad (3.23)$$

$$L = \frac{BH}{\cos \theta} \quad (3.24)$$

Equation 3.30 refers that “R<sub>pinch</sub>” is the seal radius at pinch point and “R” is the seal inner radius, which is equal to rotor radius for line-to-line condition.

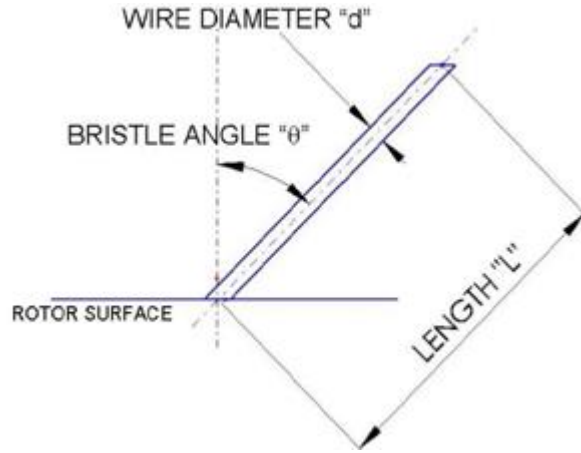


**Figure 3.2: Bristle diameters for unwrapped geometry [35]**

Duran [35] stated that bristle height should be updated as it differs from calculations that are shown below. The reason of correction comes from representation of the seal inner and outer diameter in two-dimensional plane. The correction rate is depended on seal radius for seal sample. As a result of mentioned difference between representations of brush in two dimensional models, bristle height has to be updated with formulation. Geometric illustration of the bristle height and length for brush seal model is shown in Figure 3.3 where ‘t’ is referred to the difference between corrected free bristle height and initial free bristle height. Updated calculations of bristle height and length are formulated in Equation 3.32, 3.33 and 3.34 as below:

$$BH_{cor} = BH - t = (R_{pinch} - t) - R \quad (3.25)$$

$$L_{cor} = L - t / \cos(\theta) \quad (3.26)$$

$$L_{cor} = BH_{cor} / \cos(\theta) \quad (3.27)$$

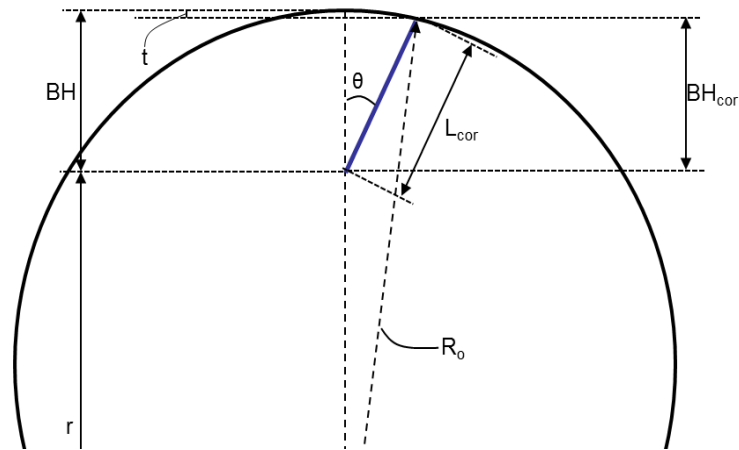
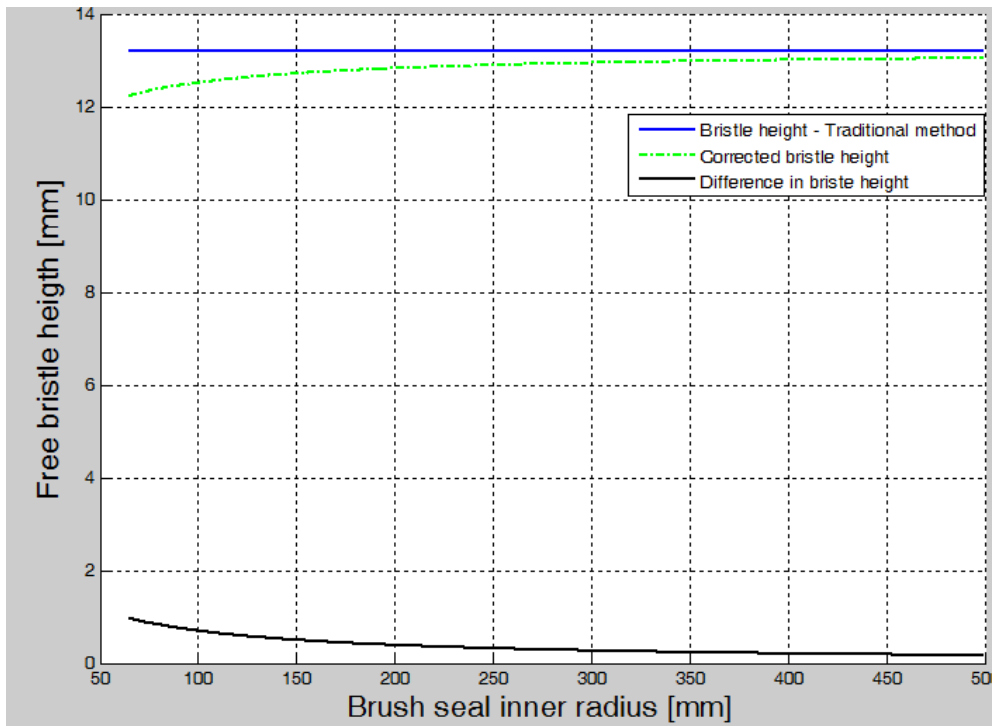


Figure 3.3: Corrected bristle height and length calculations [35]

<b>Bristle Height Correction</b>		
<b>Representative Seal, Cant Angle = 45°, Comparison for R=5.1 inch</b>		
<b>Bristle Height</b>	Free bristle height, [mm]	13.208
	Corrected bristle height, [mm]	12.241
	Difference %	7.3

Table 3.1: Bristle Height Correction

Figure 3.4 illustrates MATLAB graph for traditional bristle height and corrected version for tested seal [35]. Free bristle height is 13.208 mm and lay angle is given as 45°. The difference between two approach increases while brush seal inner radius decreases. Updated bristle height is %7.3 less than free bristle height at 5.1 in seal inner radius, which is correlated with test rig rotor and brush seal inner radius. Applying corrected version of bristle height is expected to yield more appropriate results for analysis, and it has direct influence on calibration of simulations with test data.



**Figure 3.4: Corrected bristle height change**

The corresponding angle for bristles is increasing while brush seal inner radius is decreasing. The representation with two methods are observed noticeably for small inner radius.

## 4 EXPERIMENTAL SETUP

Dynamic leakage flow tests have been performed to determine the actual leakage rate. A special test system has been used to determine leakage rates under different pressure conditions. During these tests, upstream pressure value has been varied up to 100 psid, and leakage flow rate is measured under various pressure loads. The tests were conducted at room temperature with seal downstream at atmospheric ambient air conditions. In order to calibrate resistance coefficients for CFD analysis, tests have been completed with pre-determined inlet and outlet boundary conditions. Figure 4.1 illustrates schematic and connections of the test rig.

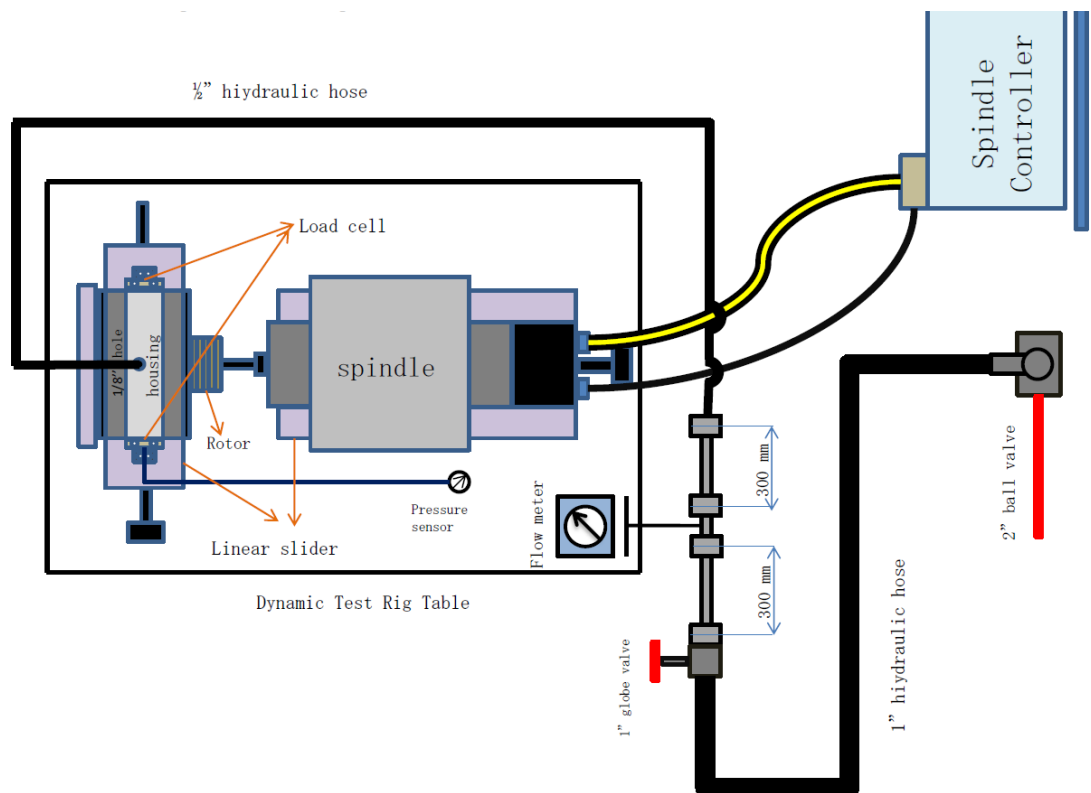


**Figure 4.1: Schematic and connections of the test rig**

The pair of brush seals are located on the rotor before starting each test. Seals are mounted on the seal housing which can be moved in the horizontal/axial direction. The position control is provided by a linear slider. Gauge pins are used to check whether the desired clearance has been achieved between rotor and backing plate. For acceptable

clearance tolerance, the seal is fixed to the housing. The upstream side of the test seals is connected to the air source. Inlet control valve sets upstream pressure and the mass flow rate is measured by a flow-meter which is located between the inlet valve and the upstream cavity of the seal. Ambient atmospheric condition which is equal to 1 bar is set to downstream region. Once test system is ready, leakage rates are measured by reading pressure difference between inlet and outlet for each test point. Upstream pressure is gradually raised to achieve up to 100 psid across the seal, and gradually decreased back to atmospheric pressure. This pressurization and depressurization cycle is repeated for three times. The raising and lowering pressure in cycles helps to capture hysteresis behavior of the seal. Leakage flow rate, upstream and downstream pressure values are measured for specified test points during each cycle. Brush seal tests have been carried out at line-to-line (no clearance and no interference between bristle pack and rotor surface) at 60 Hz rotor speed. The average value of the mass flow rate is considered for calibration in CFD analyses. Test seals have 2500 [bristles per inch] density. Post-test analyses provide the leakage rates and effective clearance values for various pressure conditions.

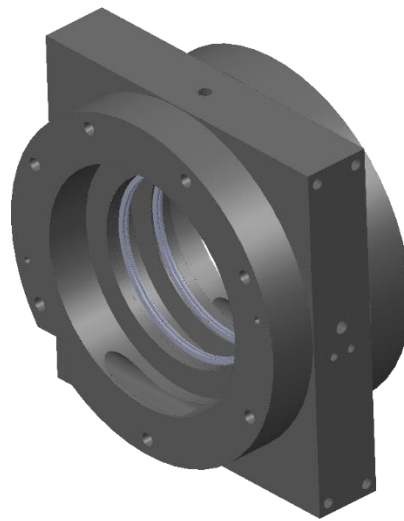


**Figure 4.2: Trimetric view of seal housing assembly**

#### **4.1 Test Rig**

Brush seal has two plates. Front plate has a gap between bristle pack to direct high pressure flow toward upper regions. Backing plate has contact with bristles in order to

increase pressure capability and leakage efficiency of brush seal. In each dynamic test, two mirror image brush seals (one left, one right) are mounted into the housing. The direction of the bristles determines brush seal as left or right. Back side of the seal is located downstream direction with atmospheric pressure. The direction of cant angle and rotation should match. O-Rings are located between cover plates and housing in order to prevent bias leakage. Therefore, air can flow only through the brush seal.

Before starting each test, the following steps are applied:

- Air is provided with a compressor which can increase pressure level up to 30 bars.
- The air is passed through a dryer to decrease wetness/humidity of the fluid.
- Ball valve is opened. Fluid moves into upstream chamber of the seals. Check for any bias leakage apart from test seal region.
- Lubrication and cooling system of spindle is activated.
- Desired pressure level is achieved by using a globe valve. Upstream pressure is checked with a digital pressure sensor.
- Leakage data is collected from flow meter. Figures 4.3-4.15 are generated according to specified upstream pressure levels.

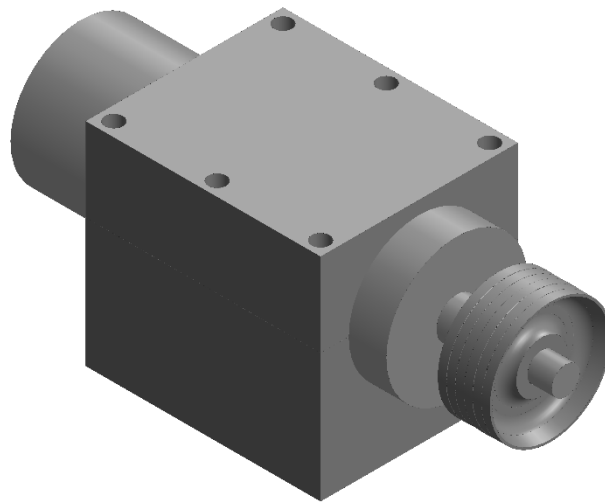


**Figure 4.3: Isometric view of rotor holder assembly**

## 4.2 Brush Seal Leakage Measurements

A set of leakage performance tests were conducted for 2500 [per/inch] bristle density test seals. Seals were tested at line-to-line conditions. The measured leakage flow rate and effective clearance levels are presented with respect to pressure difference on Figures 4.3 through 4.15. Three different test cycles are conducted, and data were averaged while generating figures. The variation of mass flow rate and effective clearance value up to 100 psid are presented for each test and seal, respectively. Cant angle has been selected as 45°, bristle diameter has been chosen as 0.1016 [mm] and fence height is 1.27 [mm]. These parameters are selected based on

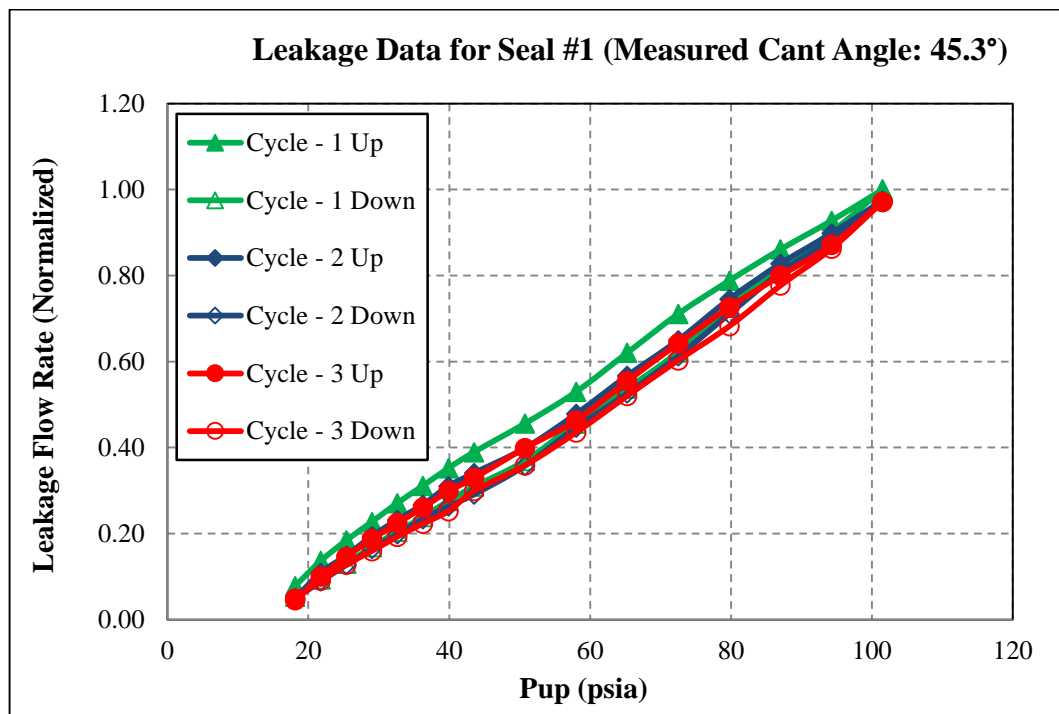


Figure 4.4: Leakage flow rate of Seal #1 for three different cycles



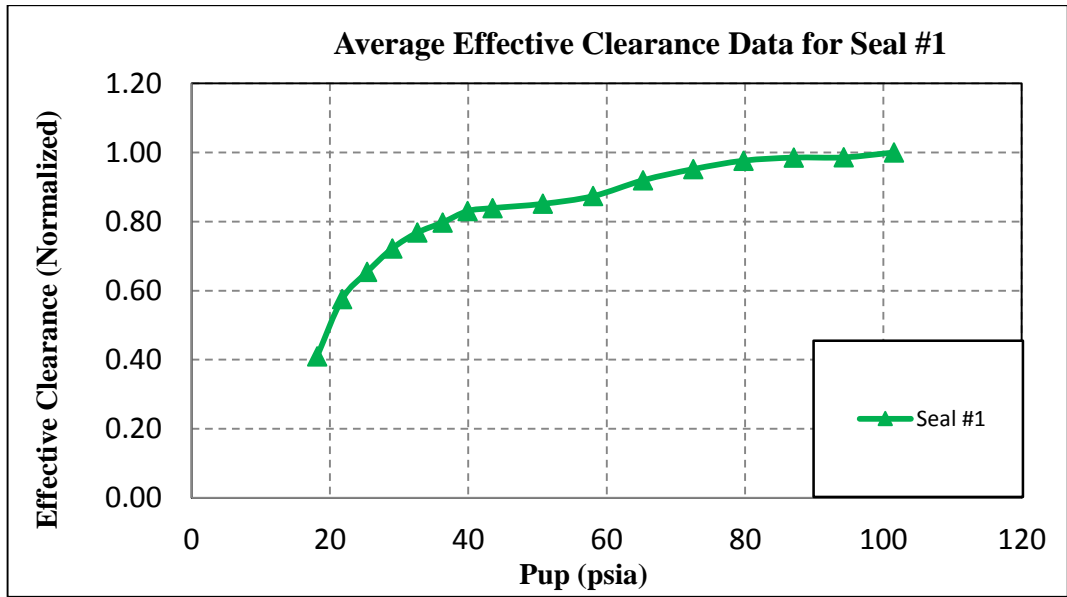


Figure 4.5: Effective Clearance of Seal #1 average of three different cycles

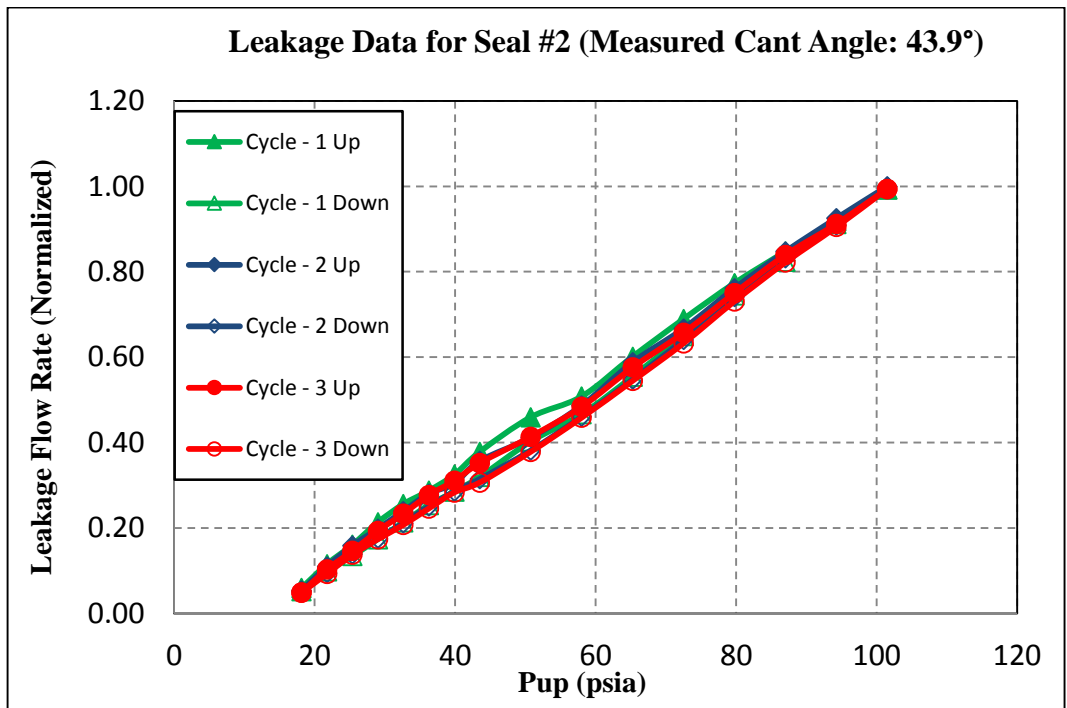


Figure 4.6: Leakage flow rate of Seal #2 for three different cycles

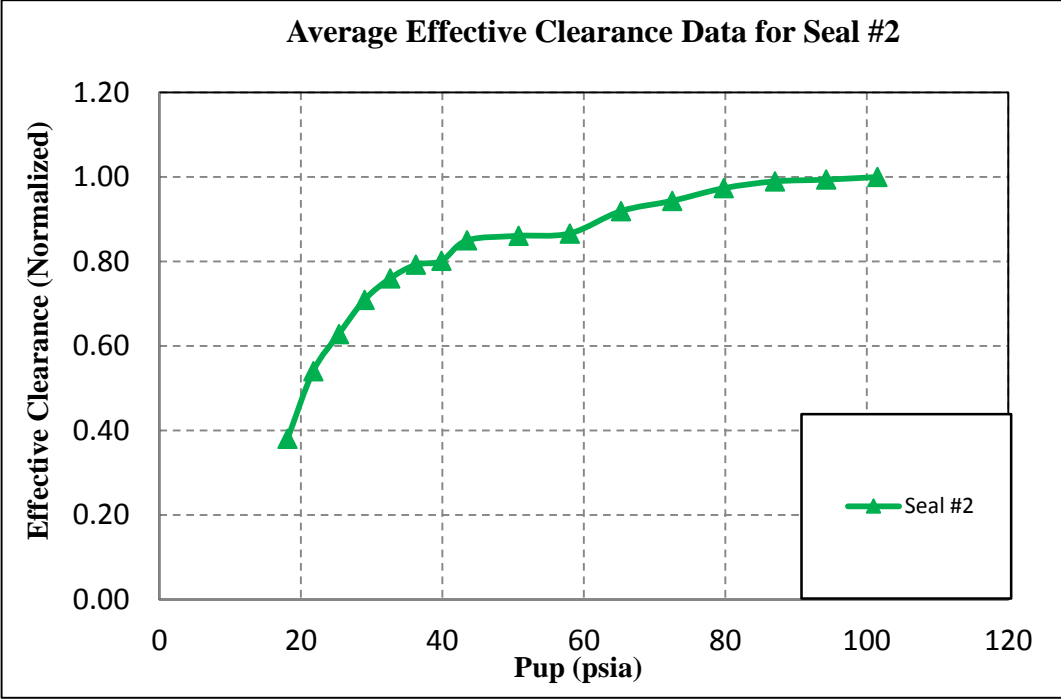


Figure 4.7: Effective Clearance of Seal #2 average of three different cycles

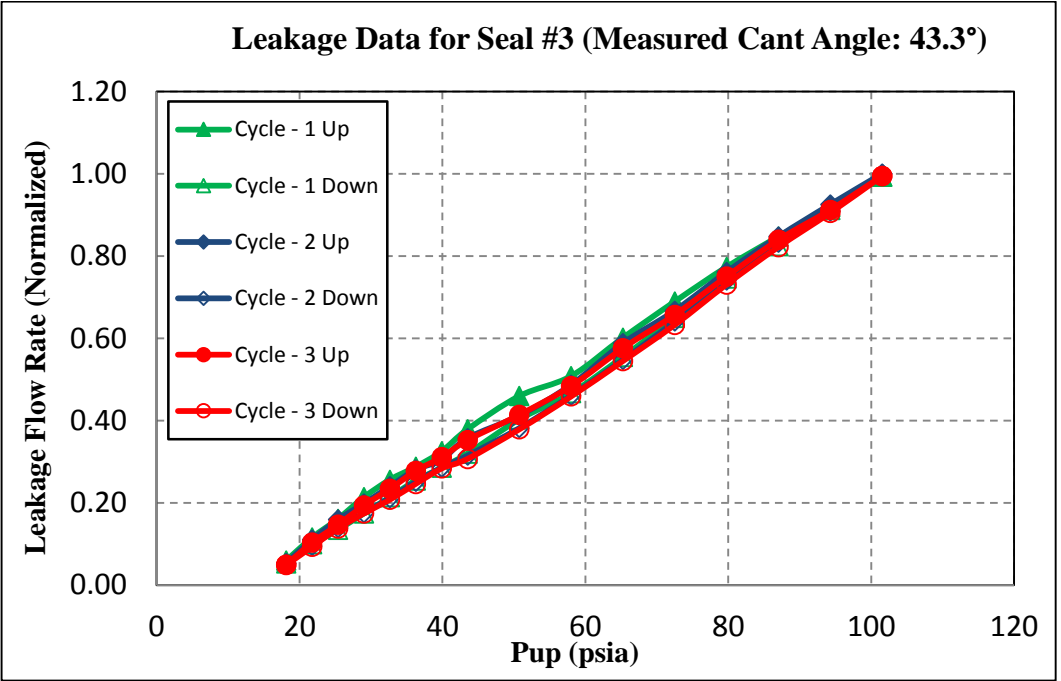


Figure 4.8: Leakage flow rate of Seal #3 for three different cycles

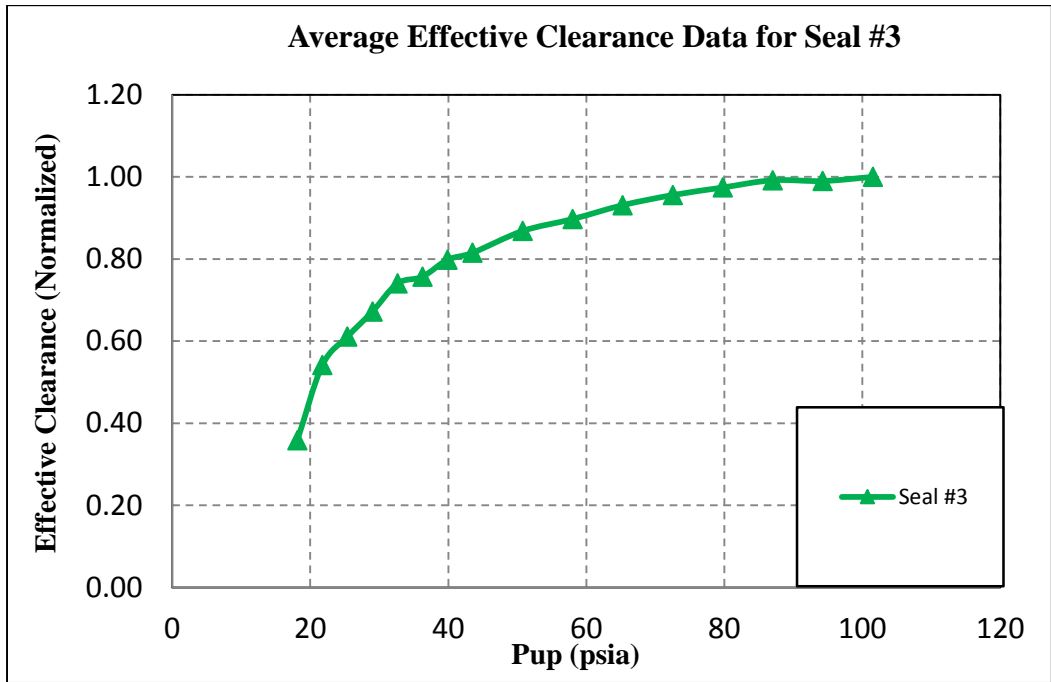


Figure 4.9: Effective Clearance of Seal #3 average of three different cycles

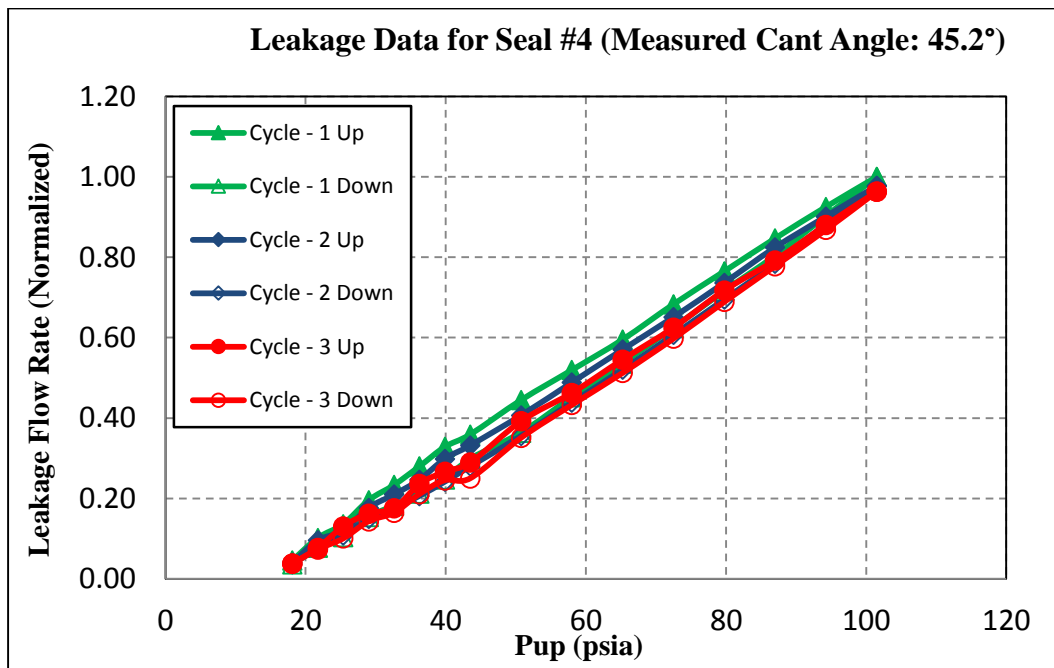


Figure 4.10: Leakage flow rate of Seal #4 for three different cycles

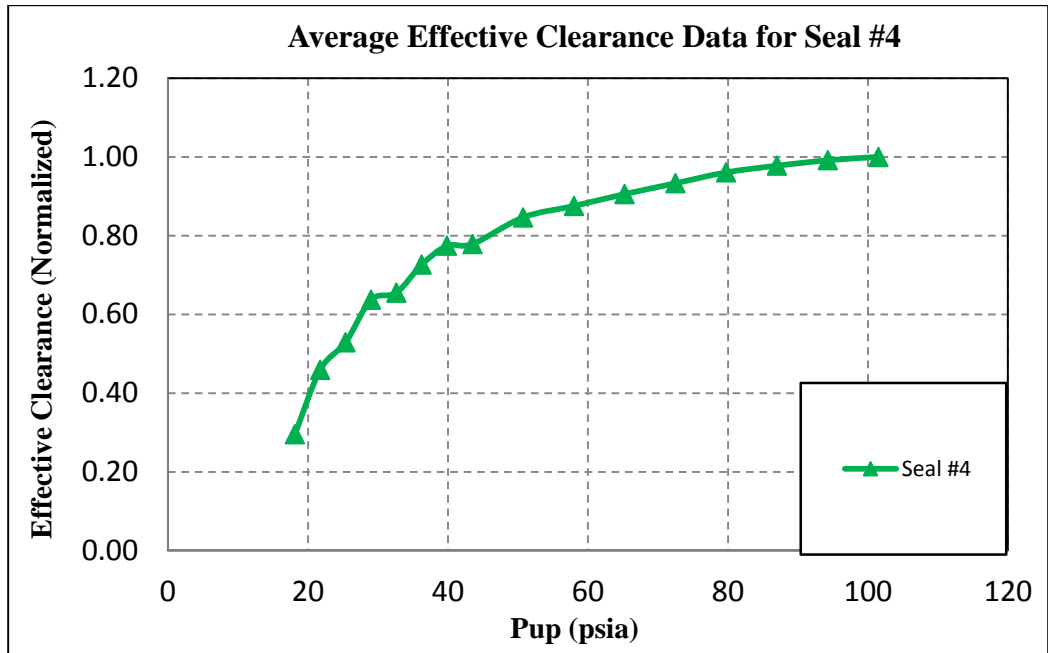


Figure 4.11: Effective Clearance of Seal #4 average of three different cycles

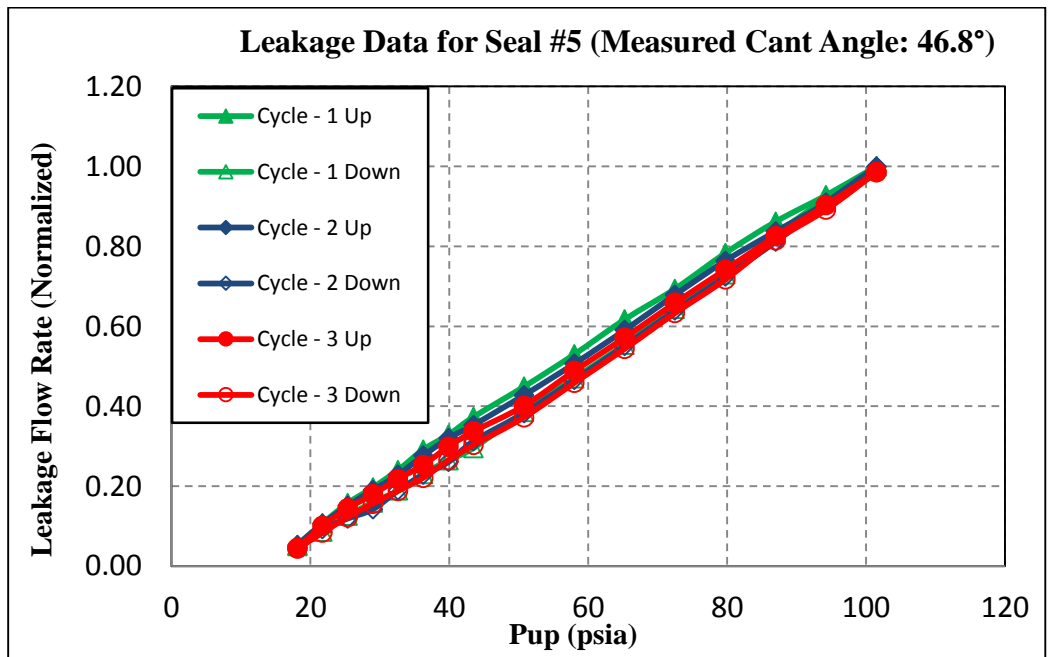


Figure 4.12: Leakage flow rate of Seal #5 for three different cycles

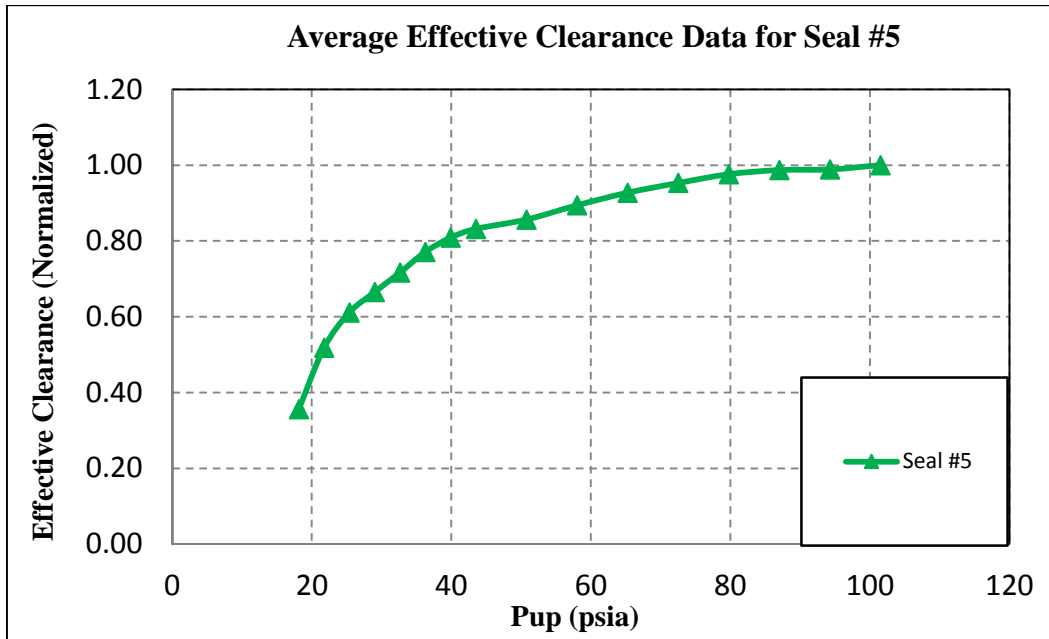


Figure 4.13: Effective Clearance of Seal #5 average of three different cycles

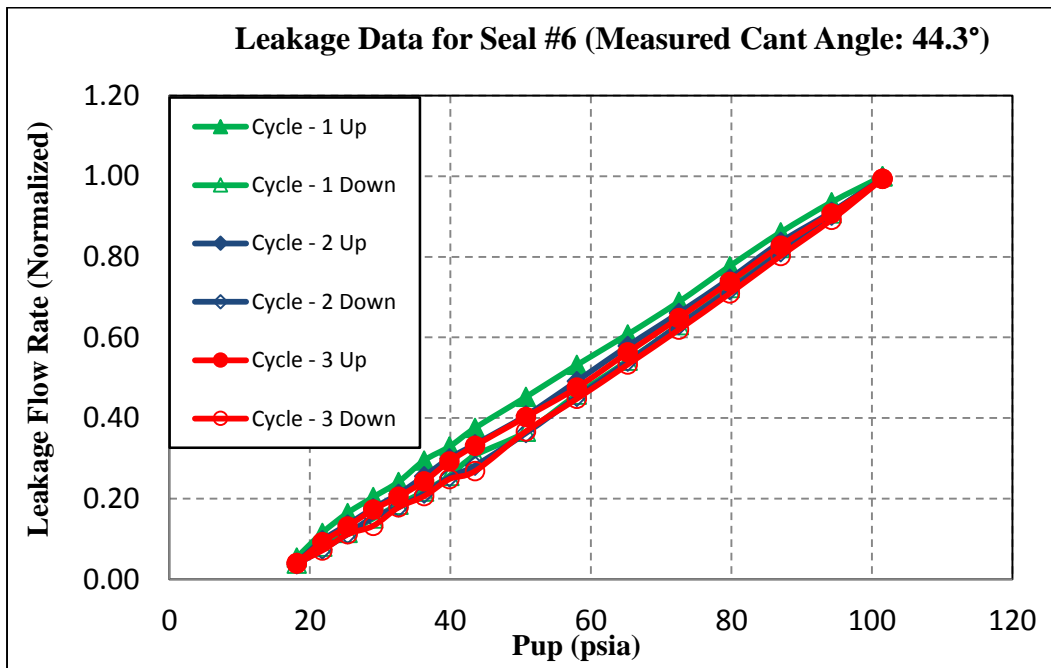


Figure 4.14: Leakage flow rate of Seal #6 for three different cycles

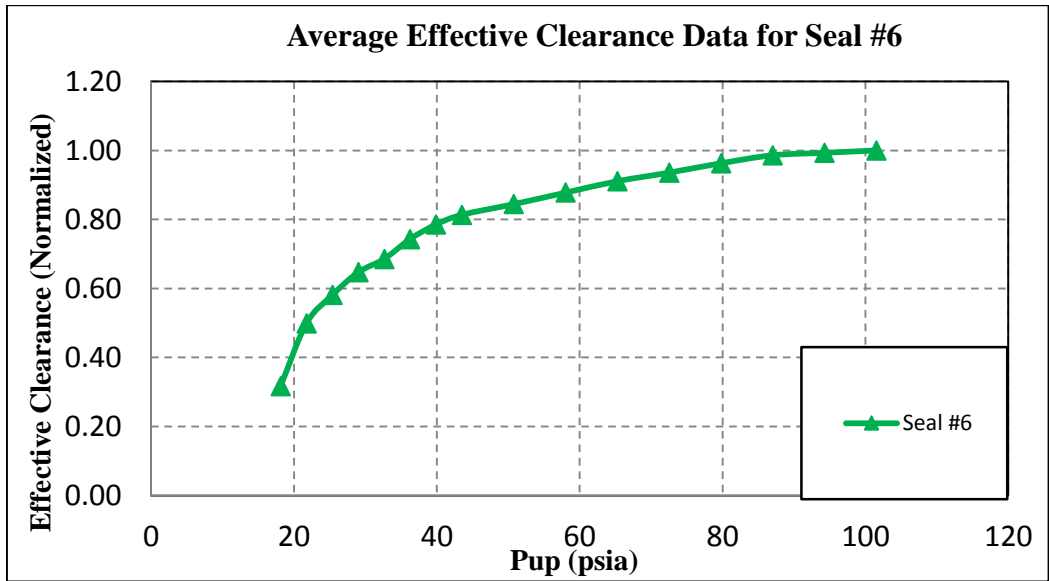


Figure 4.15: Effective Clearance of Seal #6 average of three different cycles

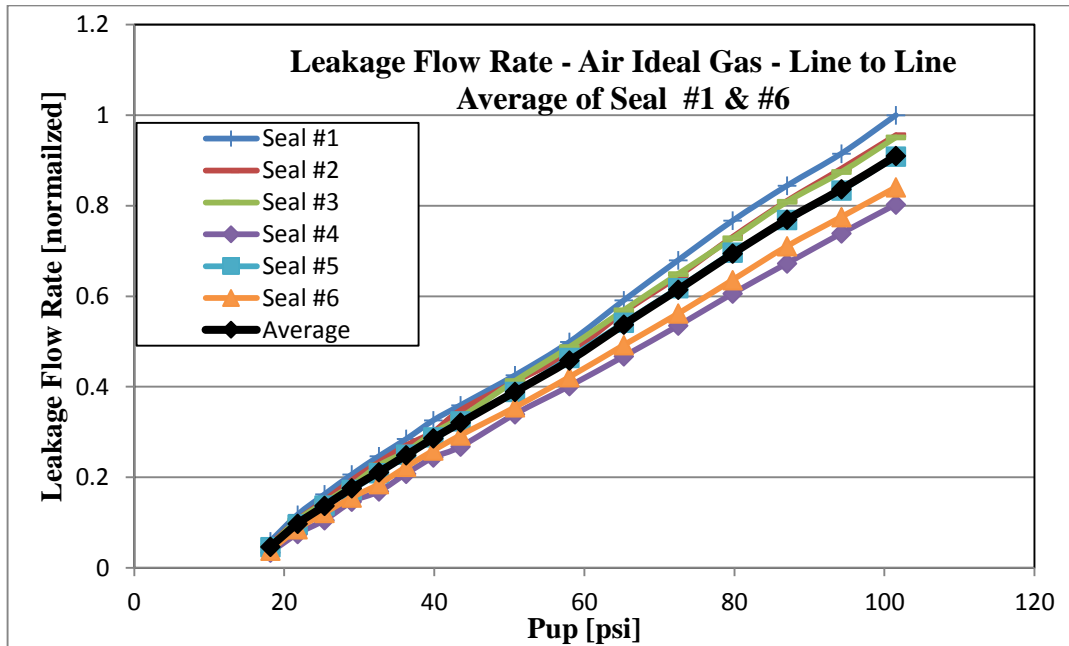
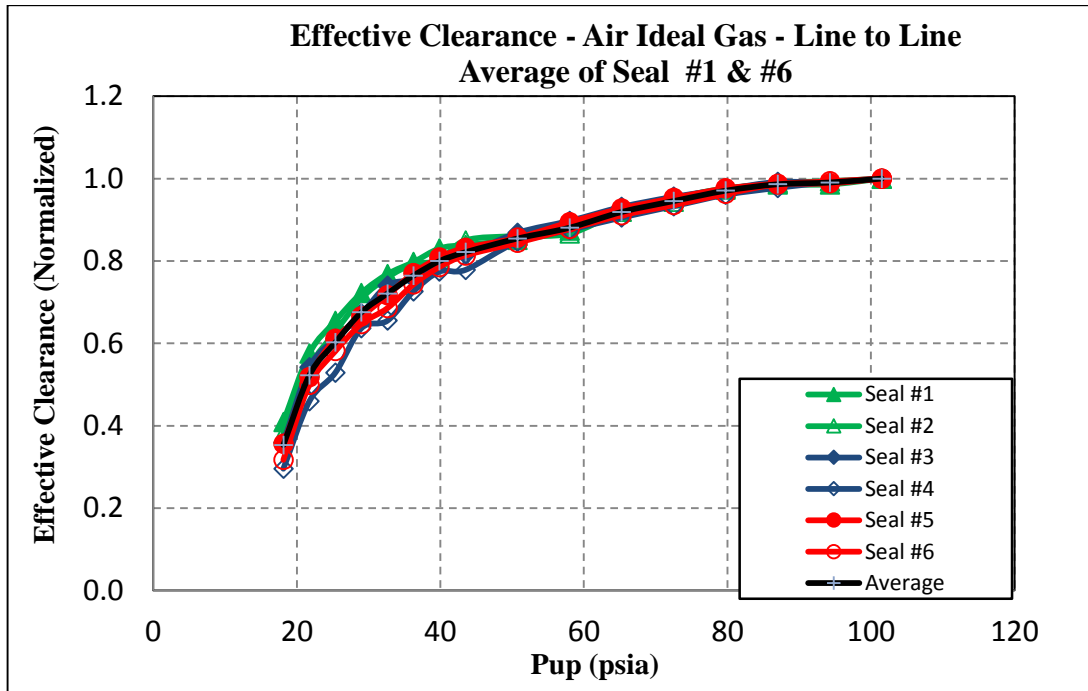


Figure 4.16: Variation of leakage flow rate for Seal #1&6



**Figure 4.17: Variation of effective clearance for Seal #1&6**

The averaged leakage rate and effective clearance has been illustrated in Figure 4.16 and 4.17. Leakage flow rate is linearly dependent on upstream pressure and pressure difference (since downstream pressure is constant). Effective clearance level has been increased dramatically for level of upstream pressure whereas it smoothly increases after  $P_{up}=50$  [psi]. Approximately, choked flow assumption is valid where pressure ratio is above 1.8. The calculation of effective clearance is changing around  $P_{up}=27$  psia.

## 5 CFD ANALYSIS OF LEAKAGE FLOW

Leakage tests are performed with air environment. The porous region resistance coefficients are calibrated with mass flow results of experiments.

### 5.1 CFD Model Using Porous Media Approach

Leakage occurs in the area between rotor and stator. As a result, brush seal is located between rotating and fixed components. Mass flow rate from upstream to downstream region is also affected by inlet and outlet pressures, and a pressure drop through the bristles. The brush seal model is divided into three main components, the front plate, the backing plate and the bristle pack (Figure 5.1). Fence height and upper brush regions are porous media components whereas the plate is considered as impervious solid in CFD simulations.

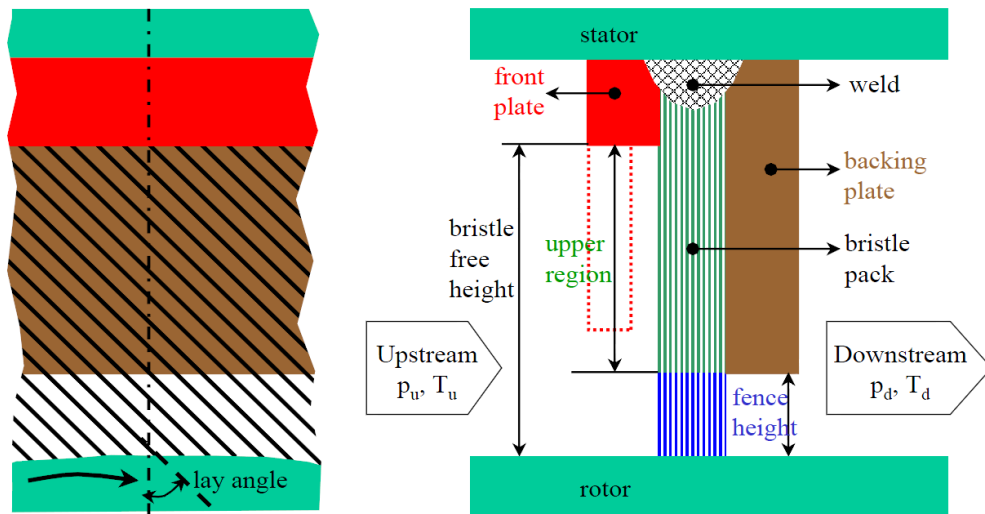


Figure 5.1: Typical brush seal geometry

CFD model is constructed for the sub-scale test rig conditions. Boundary conditions are matched to the test system. The geometry is checked with inspection of brush seals and clearance measurements. CFD estimated leakage rate is matched by iteratively by calibrating the porous medium resistance coefficients for the bristle pack. The average leakage rate of six brush seals is used in the current CFD work for three different upstream pressure values. The main objective of the calibration CFD analyses is observing

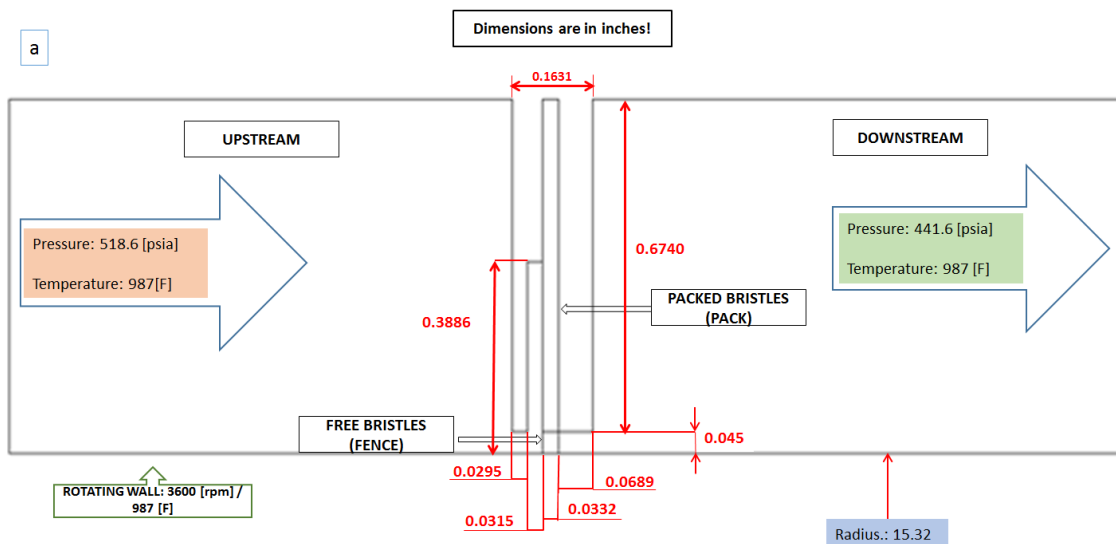


identifying porous media resistance coefficients. The porous media resistance coefficient calibration methodology is presented stated in Chapter 3. Based on Darcy Law, Equation 3.23 reveals that the flow resistance coefficients are function of pack thickness, averaged pressure across the bristle pack, temperature, pressure difference between upstream side and downstream side of porous region.

## 5.2 Boundary Conditions

As shown in Figure 5.2, bristle pack regions, upstream and downstream regions of the seal are represented in the CFD model. CFD models are simulated in ANSYS CFX commercial tool. The fluid interfaces of rotor and stator surfaces are modeled as bottom and top walls respectively. In order to minimize effects of upstream and downstream cavities, lengths of inlet and outlet regions are axially extended to three times of the brush seal radial height.

The governing equations are elaborately explained in previous chapters. Details of the computational modeling and the bulk porous medium approach are defined in this section.



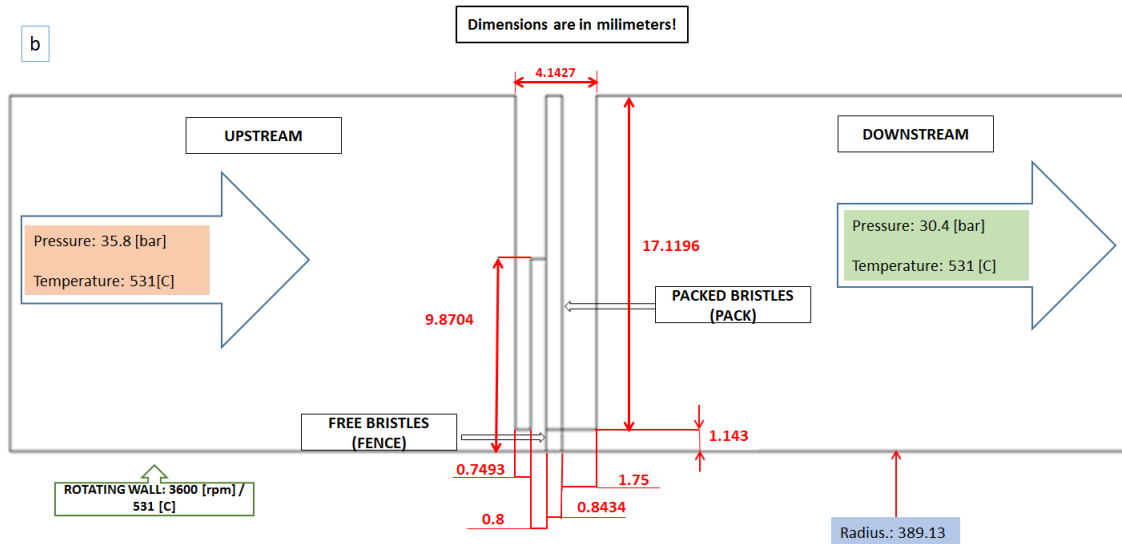


**Figure 5.2: Brush Seal Design #1 CFD Model a) Dimensions are inches b) Dimensions are millimeters**

The model is defined in 2-D axially symmetric coordinate system. As a result of cyclical symmetry in tangential direction, small angular section of the seal is selected to be modeled in order to decrease number of elements and analysis time. Experience show that two-cell thickness is adequate to observe velocity and pressure profiles.

The working fluid is air in empirical calibration cases once the resistivity coefficients are calibrated design of experiments and optimizations has been conducted for steam turbine operating conditions. The fluid is assumed as compressible and turbulent, and k-epsilon approach is selected for turbulent flow since it is robust, easy to implement, computationally cheap, good agreement for high Reynolds numbers. The air density is expressed in terms of pressure and temperature applying ideal gas law. Dynamic viscosity, specific enthalpy, specific entropy and thermal conductivity are considered at mean temperature and pressure.

Heat transfer around walls has been ignored, therefore, stator and rotor walls are modelled as adiabatic. No slip wall condition has been applied. In order to extend analysis capability for steam Peng Robinson Dry Steam is applied as ambient fluid. Viscosity, conductivity and heat capacity are calculated based on kinetic theory which are integrated into CFD calculations. Molar mass, acentric factor, critical temperature, critical pressure and critical volume are determined per Peng Robinson model.

During both calibration and steam analyses, bristle pack is considered as porous medium with specific flow resistance coefficients. The inlet and outlet is defined as open boundaries at static pressures and temperatures which are consistent with test conditions.

The effect of rotation under bristle pack area is also studied to understand dynamic characteristics of flow under turbine operating conditions. Geometrical configuration and boundary conditions are illustrated on Figure 5.2 and Table 5.1-5.2.

To capture flow details, the mesh is refined around the brush seal pack and fence height region. The iterative solution provides the appropriate values of anisotropic resistance coefficients for air environment (*Table 5.2*). The stream-wise coefficients define how much flow is resisted in the bristle pack, and dominates the axial pressure gradient as well as leakage. The transverse coefficients are dominant on controlling the flow and pressure gradient in the radial direction. Two permeable regions are fence height domain which is open to axial leakage and upper pack domain along the backing plate. Previous studies state that pack region flow resistance coefficients are 20-25% higher than the fence height region [36].

### **5.3 The Mesh**

The meshing stage has been completed using a commercially available finite element pre-processor code Hypermesh™. Free bristle height, pack thickness, fence height, rotor interference, front and backing plate thickness may vary in each design. Therefore, mesh has been updated, deleted and duplicated for different designs. Generated three dimensional mesh includes upstream, downstream, fence height, brush pack and clearance (for only clearance cases) regions. The interface between fence height and upper brush pack region has been defined as porous-porous interface. Porous-fluid interfaces have been identified between upstream-brush pack, upstream-fence height, and downstream-fence height surfaces. Additionally, fluid-fluid interfaces have been defined for upstream-clearance and downstream-clearance surfaces for clearance operation cases. The total number cells in the mesh is around 180,000 and the total number of nodes is around 275,000. Mesh is especially refined at fence height region in order to capture flow details at the most critical region in terms of leakage rate. Typical mesh is presented in Figure 5.3. For upstream and downstream region, the element size is gradually decreasing

in the close vicinity of porous domain. Mesh is also denser on the near the upper walls to solve wall function by decreasing  $y^+$  value.

In a typical mesh topology illustrated in Figure 5.3 the maximum cell size is approximately 0.3104 mm and the minimum cell size is on the order of 0.0254mm which is around the fence height region. Since the model is cyclically symmetric, two cells are included in the tangential direction. The angular section is taken as  $0.0124^\circ$  for an acceptable aspect ratio in three dimensions. All models have been created with first order hexa-mesh where maximum aspect ratio is 8.15 and maximum mesh angle is  $102.53^\circ$ . GGI (General Grid Interface) connection is applied to overlap mesh section with each other while various geometry is created.

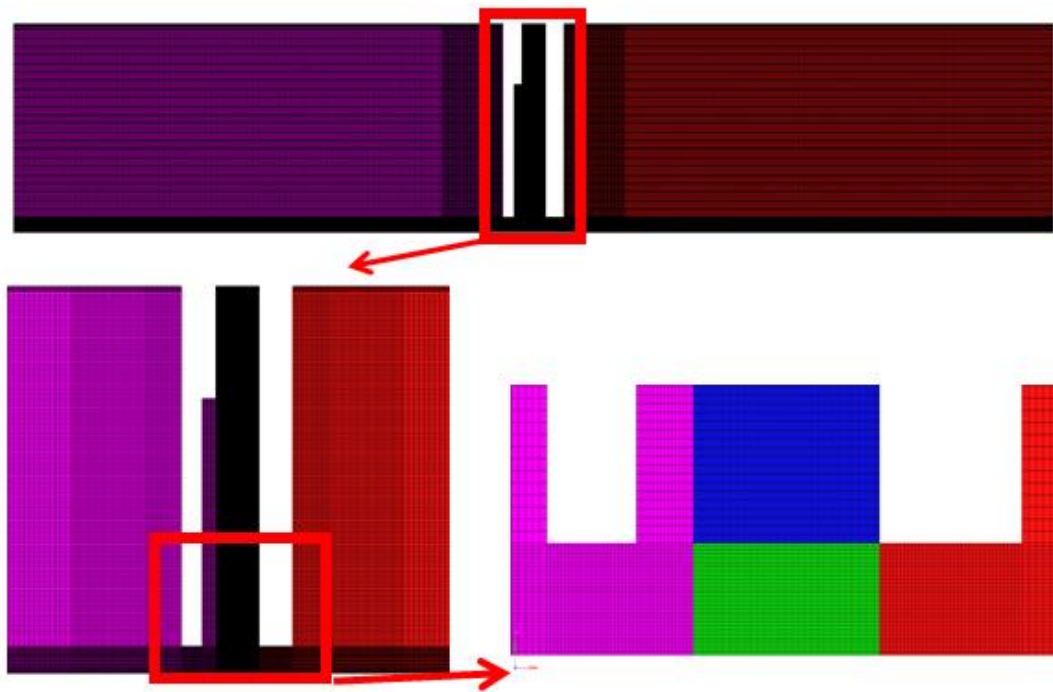


**Figure 5.3: Typical brush seal mesh for CFD analysis**

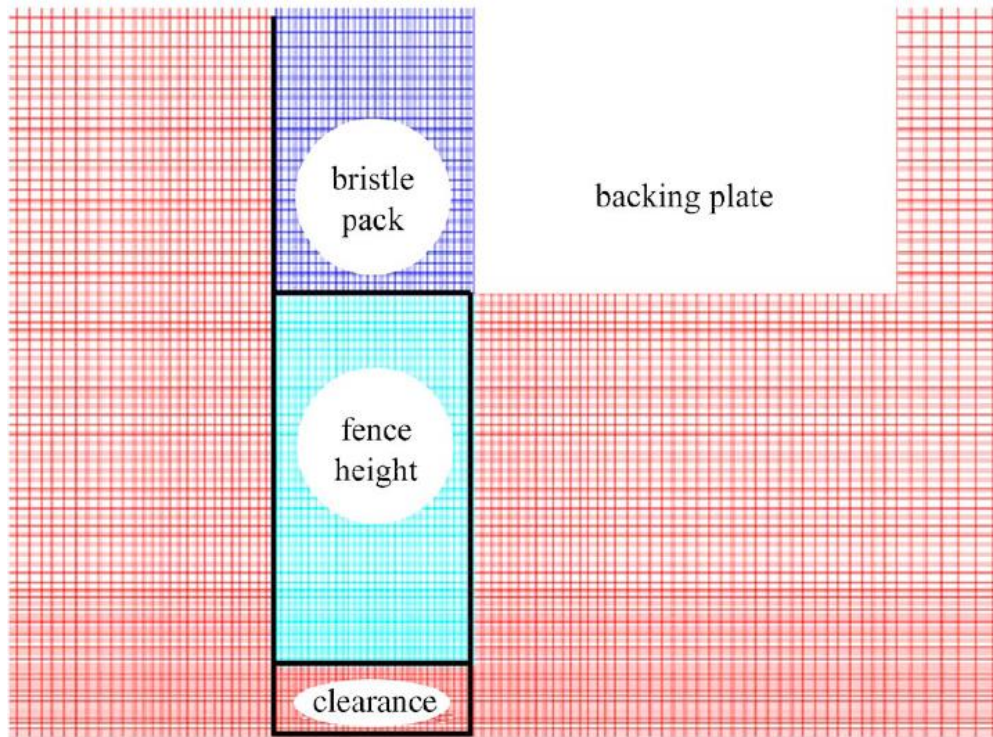


Figure 5.4: Sample brush seal meshing from literature [18]

#### 5.4 Calibration of Resistance Coefficients with Experimental Results

The matching of the calibration test results for six brush seals with CFD model calculations provided tuning of the porous media flow resistance coefficients and verification of analytical studies. The experiments have been conducted using dynamic test rig and static air test setup as explained in Chapter 4. Bristle pack material is Haynes-25 while rotor is made from stainless steel. Normalized mass flow rates and normalized effective clearance values are given in Figure 4.3 through 4.15. CFD analyses have been performed to calibrate the linear and quadratic flow resistance coefficients for the fence height and brush pack regions. Three different upstream pressure levels are selected for calibration process.

Cant Angle	Rotor Speed	Clearance	$\Delta P$ [bar]	Fluid	Volume Porosity	Bristle Density [per inch] (permm)	Rotor Dia. [mm]	Corrected BH [mm]	Min. Pack Thickness [mm]	Inlet Temp [F]	Outlet Temp [F]
45°	Static	Line-to-Line	1.05	Air Ideal Gas	0.1264	2500(98.42)	129.54	12.11	1.372	77	77
			3.44								
			5.5								

Table 5.1: CFD analysis cases and related model parameters

$\Delta P$ [psi]	Fence region resistance coefficients				Pack region resistance coefficients			
	Streamwise Linear [kg/(m <sup>3</sup> *s)]	Streamwise Quadratic [kg/(m <sup>4</sup> )]	Transverse Linear [kg/(m <sup>3</sup> *s)]	Transverse Quadratic [kg/(m <sup>4</sup> )]	Streamwise Linear [kg/(m <sup>3</sup> *s)]	Streamwise Quadratic [kg/(m <sup>4</sup> )]	Transverse Linear [kg/(m <sup>3</sup> *s)]	Transverse Quadratic [kg/(m <sup>4</sup> )]
15	4,262	4,262	362,228	362,228	5,114	5,114	1,022,760	1,022,760
50	9,902	9,902	841,672	841,672	11,882	11,882	2,376,485	2,376,485
80	15,272	15,272	1,298,151	1,298,151	18,327	18,327	3,665,367	3,665,367

**Table 5.2: Calibrated resistance coefficients**

Resistance coefficients are integrated models intuitively. After solutions has been converged, the values of resistance coefficients has been manipulated to reach same values gained from experimental data. Table 5.2 illustrates fence and pack region resistance coefficients for calibrated resistance coefficients with test results. Resistance coefficient values are proportionally increased with respect to pressure difference due to bristle stiffening effect. Normalized values of test and CFD results have been shown in Table 5.3.

Clearance State	Ambient	$P_{up}$ [bara]	$P_{down}$ [bara]	$\Delta P$ [bard]	Pressure Ratio	Test		CFD	
						$m$ [Normalized]	Effective Clearance [Normalized]	$m$ [Normalized]	Effective Clearance [Normalized]
Line-to- Line	Air Ideal Gas	2.05	1	1.05	2.04	0.2271	0.7147	0.2151	0.6767
		4.44	1	3.44	4.21	0.6497	0.9497	0.6386	0.9334
		6.5	1	5.5	6.46	1.00	1.00	1.00	1.00

**Table 5.3: Calibration of averaged mass flow rate and effective clearance between test results and CFD**

## 5.5 Verification of Porous Media Resistance Coefficients with Ideal Gas Approach

The model verification process involves the actual task of predicting resistance coefficients for various pressure difference levels, and verifying the analytical results through leakage tests. The experiments have been correlated with CFD analysis as described in Chapter 5.4. Three different CFD models have been constructed with boundary conditions given in Table 5.1 and 5.3. Analytically estimated and iteratively calibrated resistance coefficients are tabulated in Table 5.4. The difference between test

results and CFD estimates does not exceed %5 in air environment. For steam ambient condition, a design of experiments is performed.

ΔP [psi]	Calibrated CFD Results with Tests				Analytical Estimation from Equation 3.24				Difference %
	Fence region resistance coefficients		Pack region resistance coefficients		Fence region resistance coefficients		Pack region resistance coefficients		
	Streamwise Linear [kg/(m <sup>3</sup> *s)]	Transverse Linear [kg/(m <sup>3</sup> *s)]	Streamwise Linear [kg/(m <sup>3</sup> *s)]	Transverse Linear [kg/(m <sup>3</sup> *s)]	Streamwise Linear [kg/(m <sup>3</sup> *s)]	Streamwise Quadratic [kg/(m <sup>4</sup> )]	Transverse Linear [kg/(m <sup>3</sup> *s)]	Transverse Quadratic [kg/(m <sup>4</sup> )]	
15 (reference point)	4,262	362,228	5,114	1,022,760	4,262	362,228	5,114	1,022,760	0
50	9,902	841,672	11,882	2,376,485	10,398	888,835	12,478	2,495,534	5.01
80	15,272	1,298,151	18,327	3,665,367	15,427	1,311,264	18,512	3,702,391	1.01

**Table 5.4: Comparison of Resistance Coefficients for Calibrated CFD Results with Tests and Analytical Estimation**

## 5.6 CFD Results

### 5.6.1 Flow Condition

Table 5.3 shows mass flow rate and effective clearance values for specified boundary conditions. Figure 5.4 illustrates velocity vectors of the fluid where the flow approaches the seal from the upstream cavity. In the vicinity of front plate, flow slows down gradually, and it slowly penetrates through bristle pack. In the upper brush pack region fluid moves into the bristles and accumulates at the backing plate interface which results in fast radially inward flow at the upstream face of the backing plate. Maximum velocity is observed around the backing plate inner corner where brush pack, fence height and downstream regions meet. Fluid moves predominantly in axial flow in the fence height region and predominantly downward radial flow in the upper brush pack region. Flow in downstream and upstream cavities are illustrated in Figure 5.5. Fluid has relatively higher velocity in the close vicinity of the interface between downstream and brush at the fence height. In this region, velocity vectors show that there is strong tangential flow in shaft rotation direction. This high flow velocity results in drag force on the bristles which may lead to bristle flutter depending on the balance of forces.

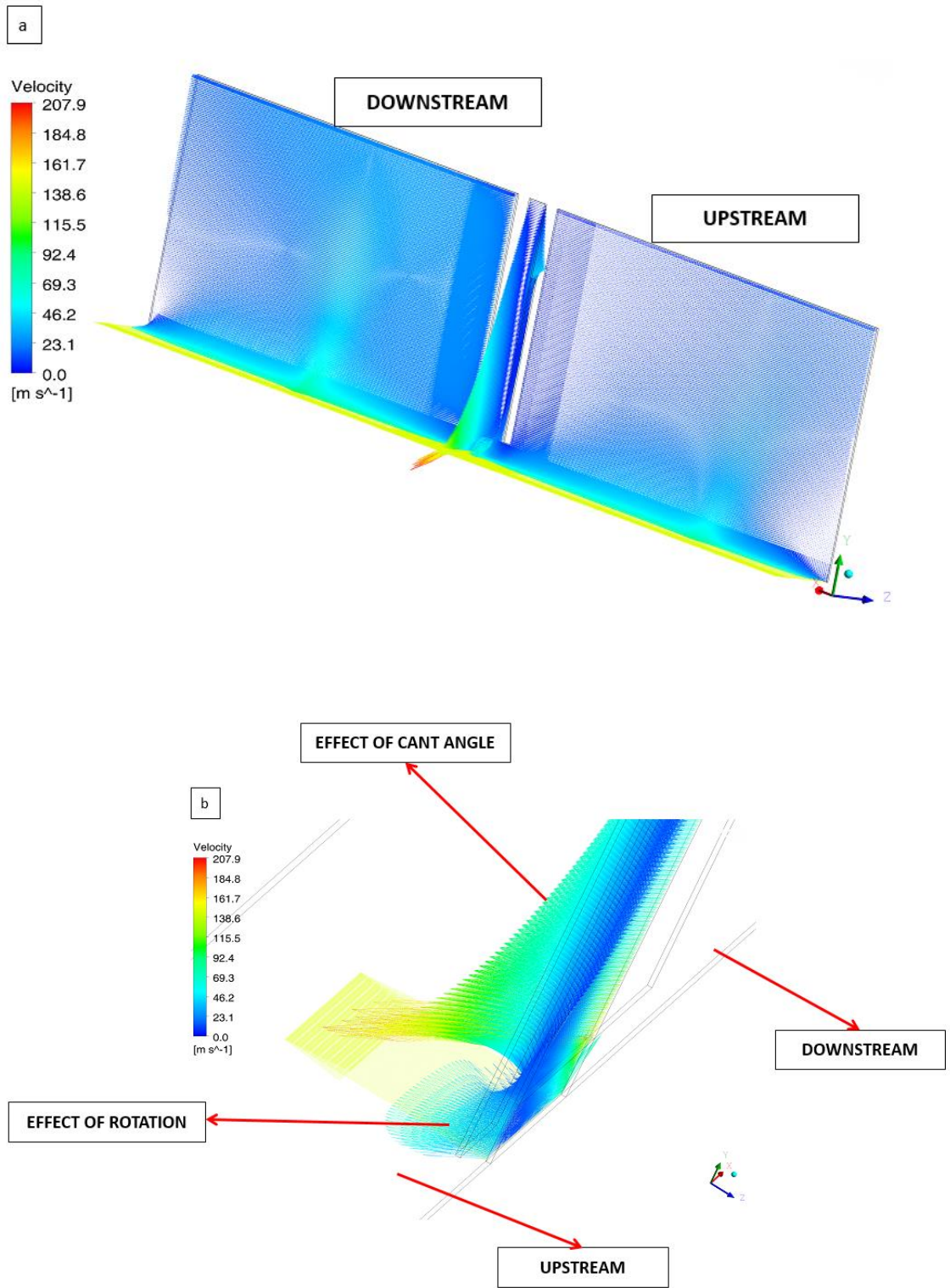


**Figure 5.5: Velocity vectors for optimal solution at turbine operating condition a) Including downstream and upstream region b) Only fence and pack region**



### 5.6.2 Velocity Profile

In Figure 5.5, the velocity streamlines are illustrated for optimal solution with calibrated flow resistance coefficients for different pressure levels.

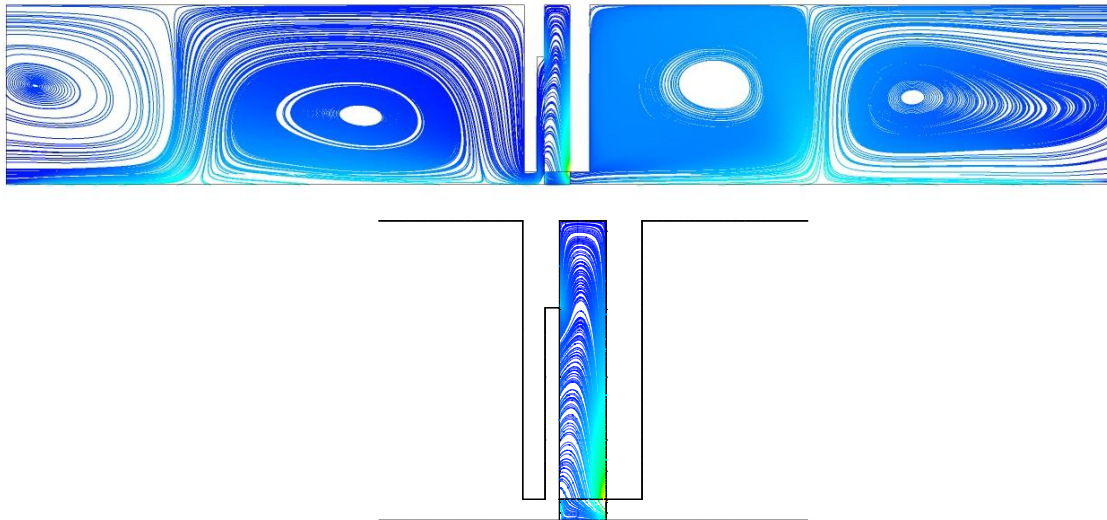
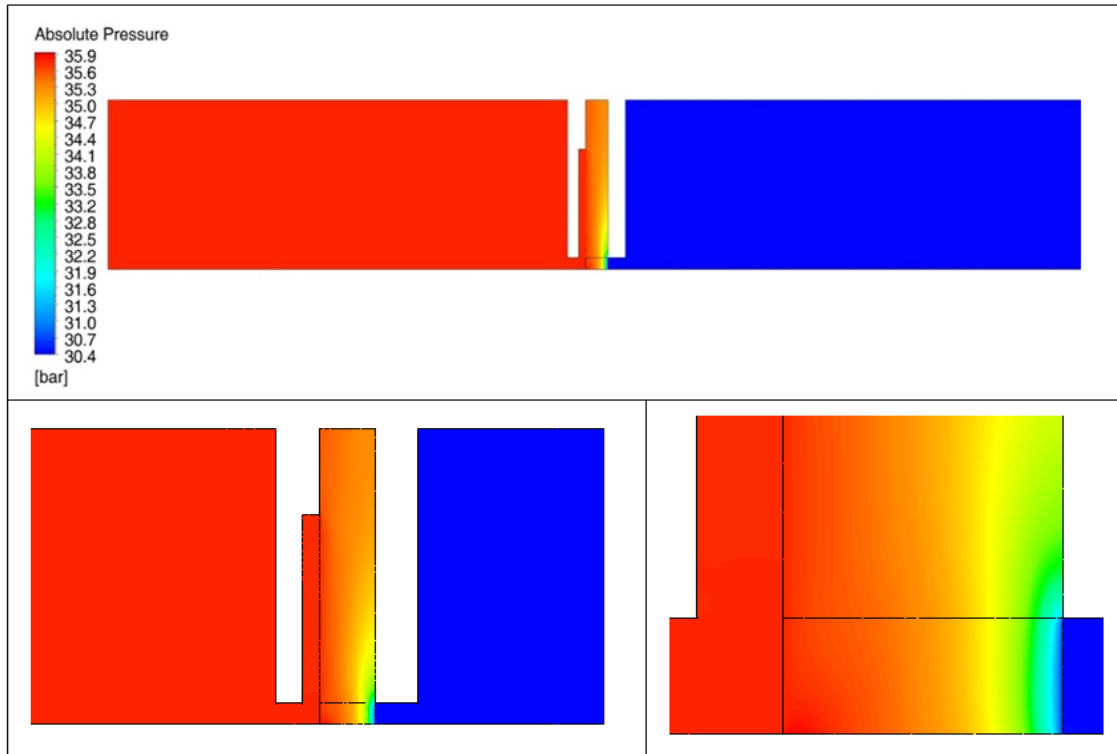


**Figure 5.6: Velocity streamlines for optimal solution at turbine operating condition**

The swirls and vortices are observed in upstream and downstream regions for given boundary conditions. The velocity of flow gradually increases when passing around backing plate corner. Flow velocity approaches Mach number at brush-rotor clearance for clearance operation cases. In addition, vortices are observed densely in clearance cases while the radius of vortices remain small.

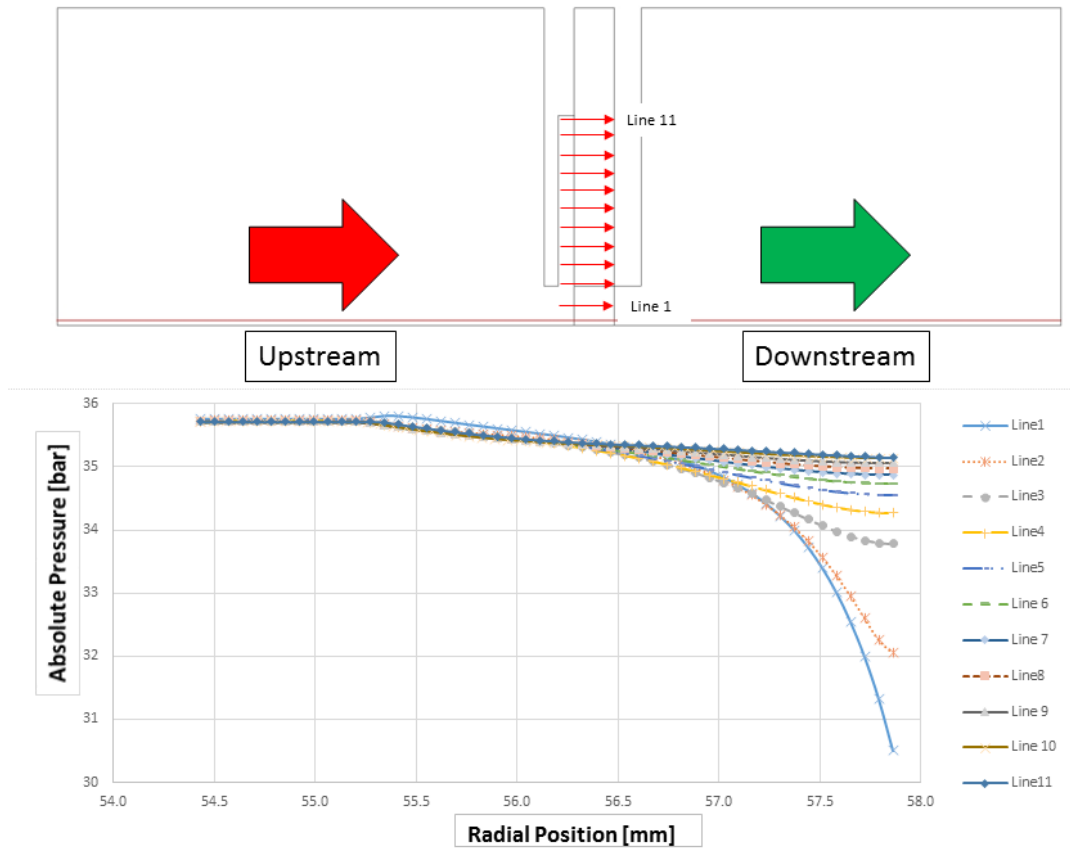
### 5.6.3 Pressure Profile

Pressure distribution is captured in Figure 5.6 where pressure is not changing considerably in the non-porous area. It dramatically decreases from the upstream region to downstream region over the brush seal pack thickness. Maximum pressure drop exists near the rotor surface of the fence height region where the main flow is moving axially through the seal.

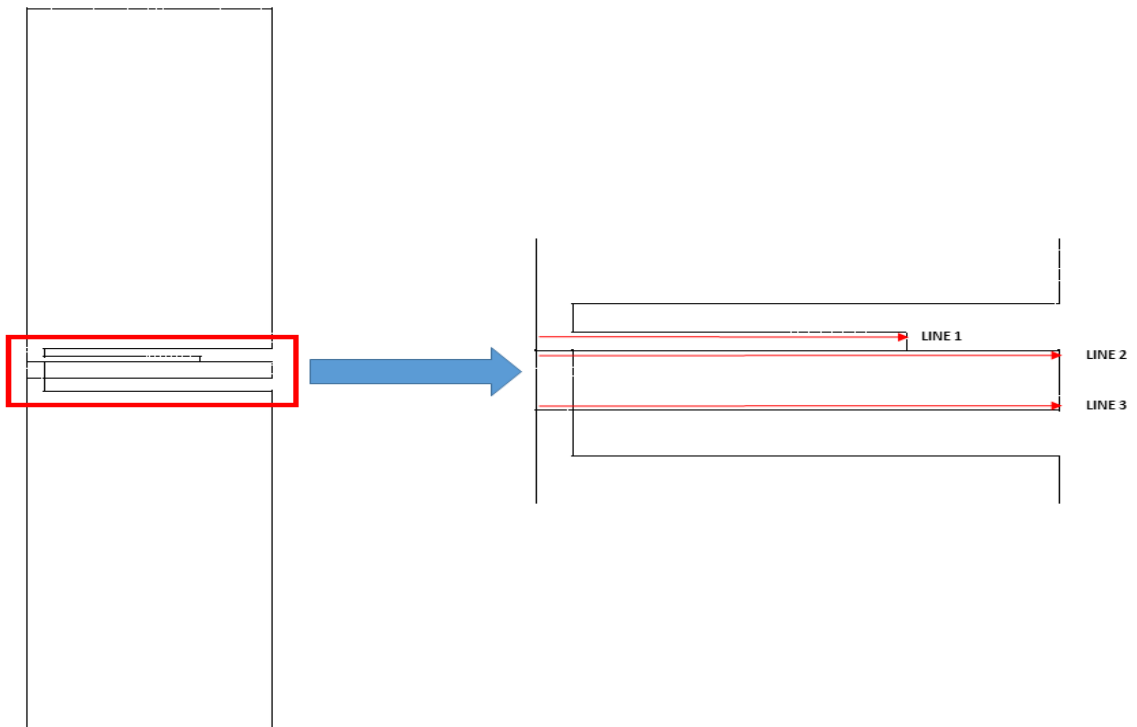


**Figure 5.7: Absolute pressure distribution for optimal solution in [bar] at turbine conditions**

Axial pressure distributions in porous domain at 11 different radial positions are presented in Figure 5.7. The pressure difference reaches maximum level around the fence region while it stays nearly constant at the upper brush pack region. The pressure lines are almost linear in the upper brush pack region whereas pressure drop profile is similar to second order polynomial in the fence height section. The pressure change is almost zero around the upper most location of bristles near welded section.



**Figure 5.8: Axial pressure distribution between front and backing plate for optimal solution at turbine operating conditions**



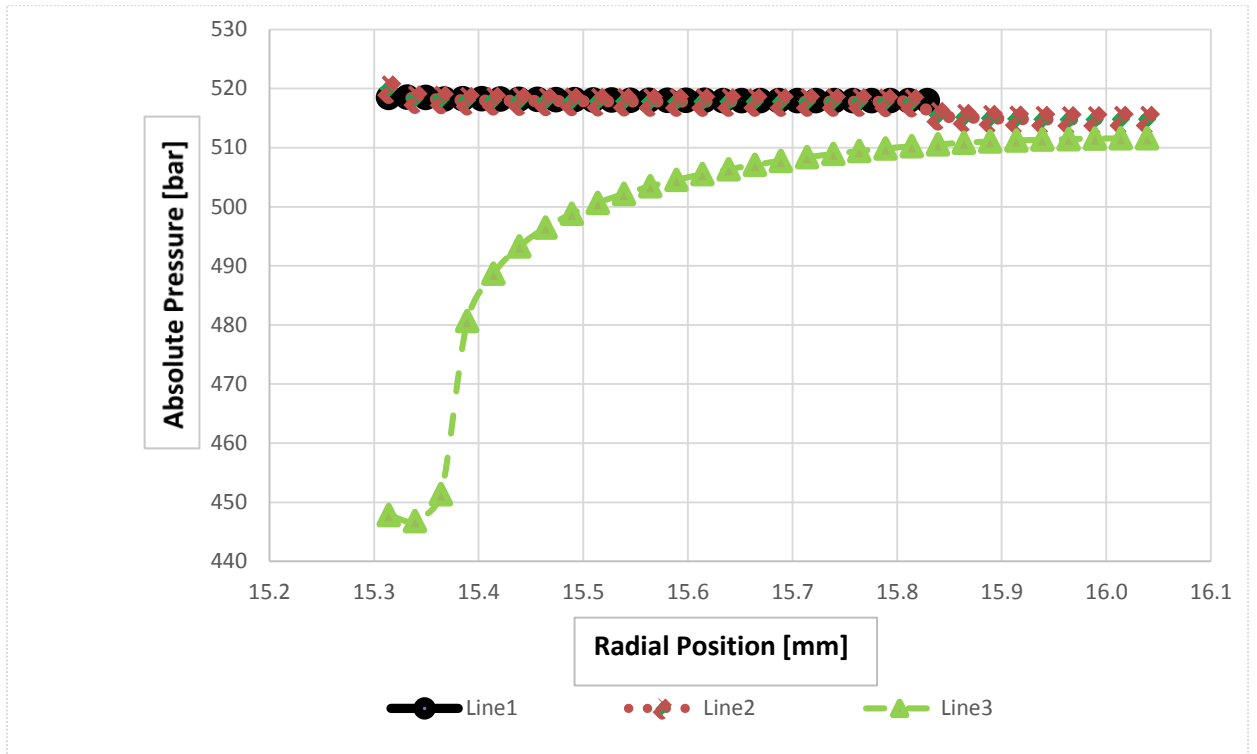


**Figure 5.9: Radial pressure distribution on front and backing plate surface for optimal solution at turbine operating conditions**

The axial pressure change from inlet to outlet is presented in Figure 5.8. and 5.9. Pressure drop is clearly observed in the porous domain. Radial pressure is changing around backing plate while it is almost steady around front plate.

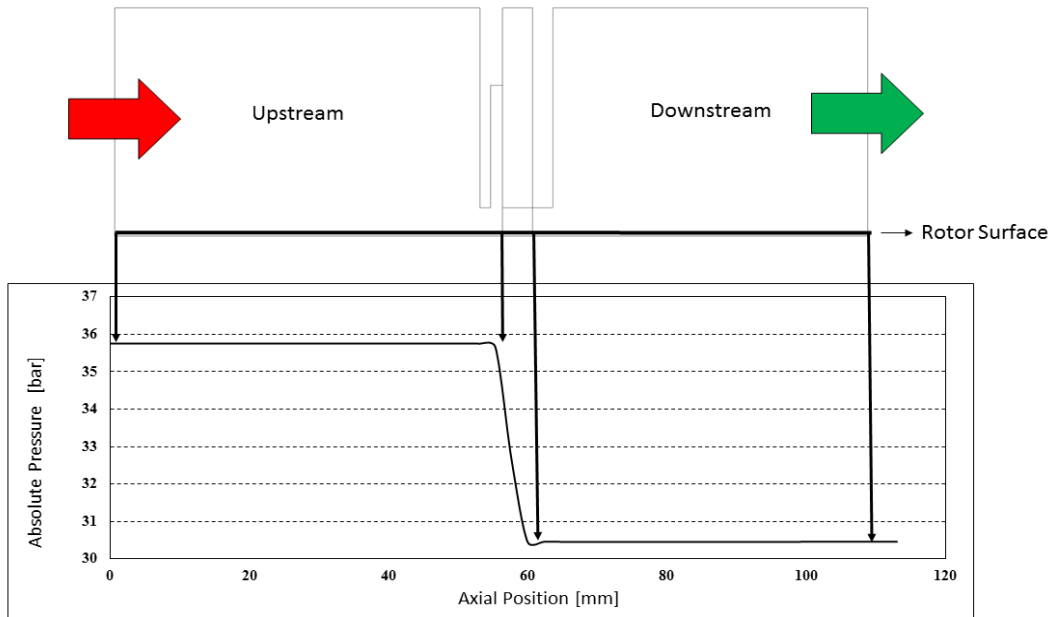


**Figure 5.10: Axial pressure distribution on rotor lower surface for optimal solution at turbine operating conditions**

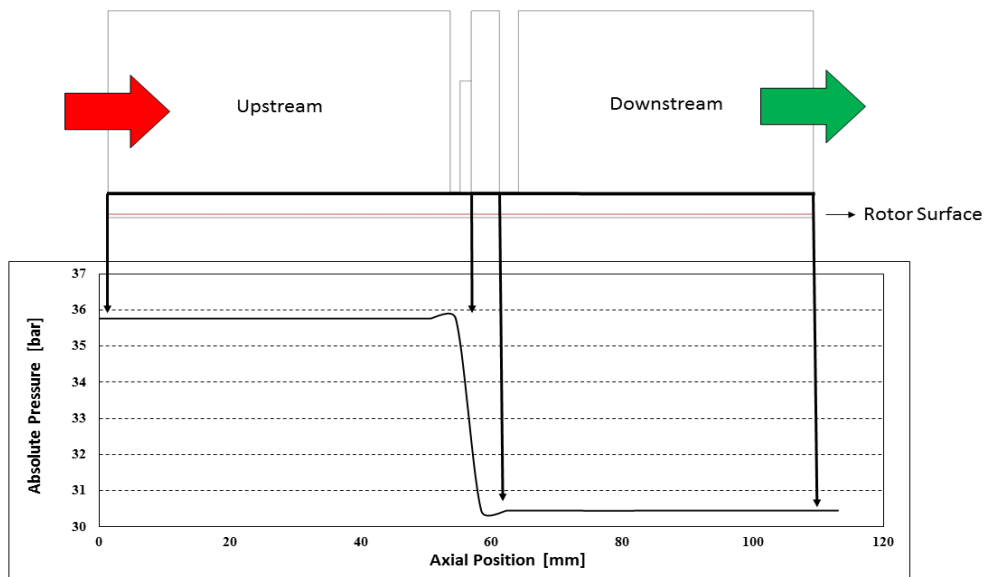


**Figure 5.11: Axial pressure distribution on rotor upper surface for optimal solution at turbine operating conditions**

## 6 DESIGN OF EXPERIMENTS

In order to understand the influence of design parameters on flow resistivity coefficients, a design of experiments study has been conducted, and presented in this chapter. Considering that there is no single formulation that can be validated for leakage performance contributing equations will be considered in order to reach an optimum design. Effective area and effective clearance of a brush seal can be calculated when leakage rate is determined. In an attempt to optimize design parameters, 18 design combinations are modeled. Applying statistical tools is beneficial to illustrate the effects of the design variables on mass flow rate. The seal design variables are treated as controllable parameters and called as ‘the factors’ while the output, which are flow resistance coefficients, are called ‘the response’. In this chapter, design optimization process is presented with the following steps.

- Determination of design variables
- Selection of appropriate test matrix
- Determine levels of factors for design of experiments
- Running CFD simulations according to design of experiments test matrix
- Deriving response equations based on simulation results

### 6.1 Brush Seal Design Variables (The Factors)

The experiments have been conducted in a manner to capture the relationship between differential pressure and leakage rate as discussed in Chapter 4. The other possible main factors are determined from previous studies. Eight other main design factors have been identified and used in experiments as listed below:

- rotor clearance
- cant angle
- free bristle height
- bristle density
- bristle diameter
- fence height

- front plate thickness
- backing plate thickness

## 6.2 Main Experiment Design

Since simulations take long time. In addition to selecting parameters that are involved in design of experiments, the most influential design variables are identified. After effect of each factor is determined, the response can be optimized using only the most influential parameters to reduce computational time. This screening process also involves a set of design experiments to cover various combinations of design variables. Simulations are performed with different levels of factors where ‘levels’ refer to the selected test values of the factors. The levels of each factor are specified based on previous studies in order to cover a reasonable work domain and to obtain realistic results. Design variables have only low and high levels for ‘two-level’ design of experiment, whereas ‘three-level’ design also includes a middle level of factors providing better response resolution.

If a full factorial experiment is conducted, every possible design combinations should be performed which requires  $2^8=256$  simulations for two-level designs. The required number of simulations rises to  $3^8=6561$  for a three-level design. As the numbers indicate, the full factorial experimental design requires very large simulation times. Therefore, it is not used in this work.

Another method is called ‘fractional factorial’ which performs less number of simulations by eliminating some combinations and investigating only some combinations. However, the disadvantage of this method is the loss of resolution. A full factorial designs yields information on main factor effects as well as factor interaction effects. Typically, interactions account for drastically more degrees of freedom (DOF) and require much more additional run combinations than just the main factors. Taguchi has developed a special set of fractional factorial test matrices that eliminate only interaction DOFs and preserve main factor effects while eliminating a large number of run combinations. Taguchi test matrices selectively eliminate some combinations in such

a way that they maintain orthogonality of the matrices. This allows unbiased evaluation of all main factors without any bias. Orthogonal arrays also allow uniform sampling of the design space in all directions. In this work, a special Taguchi orthogonal array of L18 has been used. This array allows for evaluation of all 8 factor effects in 3 levels without any bias from interactions.

Level Values of Factors							
Factor Name	Label	High	Middle	Low	High	Middle	Low
Rotor Clearance	A	0.1524 [mm]	0.0762 [mm]	0 [mm]	6 [mil]	3 [mil]	0 [mil]
Cant Angle	B	55°	45°	35°	55°	45°	35°
Free Bristle Height	C	15.24 [mm]	13.2 [mm]	10.16 [mm]	600 [mil]	520 [mil]	400 [mil]
Bristle Density	D	98.43 [per mm]	83.66 [per mm]	68.89 [per mm]	2500 [per inch]	2125 [per inch]	1750 [per inch]
Bristle Diameter	E	0.127 [mm]	0.1016 [mm]	0.0762 [mm]	5 [mil]	4 [mil]	3 [mil]
Fence Height	F	1.905 [mm]	1.524 [mm]	1.143 [mm]	75 [mil]	60 [mil]	45 [mil]
Front Plate Thickness	G	1.25 [mm]	1 [mm]	0.75 [mm]	50 [mil]	40 [mil]	30 [mil]
Backing Plate Thickness	H	2 [mm]	-	1.75 [mm]	80 [mil]	-	70 [mil]

**Table 6.1: Level values of factors**

The simulations have been executed using the factor levels described in Table 6.1. The maximum and minimum dimensions of the mesh elements are mentioned in Chapter 5. Although geometry of the brush seal varies for each experiment, mesh size does not exceed the specified limits of the mesh dimensions.

The performed Taguchi optimization method investigates the effect of selected factors over response. It is straightforward and simple to apply for the selected levels of parameters. The selected L18 array has a critical advantage by distributing interaction effects equally. Once the simulations have been completed strong and weak factors have been determined using Pareto Chart, and optimal combinations have been determined. The significance of factors is displayed in Pareto Chart. The main effect charts reveal the trend of response for each factor.



Once the leakage rates are obtained, effective area and clearance can be estimated by applying Equations 3.28 and 3.29. The results for estimation resistance coefficients are tabulated respectively in Table 6.3 and 6.4 based on ideal gas approach and quadratic interpolation of pressure difference.

### 6.3 Design of Experiment Results for Ideal Gas Approach

As described in Chapter 3, porous media resistance coefficients are calibrated by applying Navier-Stokes, Darcy Law and Ideal Gas Law to the brush seal model. Equation 3.24 is used in the model in order to allow resistance coefficients to change in each iteration simultaneously. One should select reference point as a bench mark case based on known previous studies. For these cases, CFD results calibrated with test data are selected as reference case. In Chapter 5, comparison of test and CFD analysis results is performed for three different pressure values ( $\Delta P=1.05, 3.44, 5.5$  bar). 5.5 bar pressure difference case has been chosen as reference point which has closest  $\Delta P$  value to some selected turbine operating conditions ( $\Delta P=5.3$  bar). Table 6.2 shows reference and CFD analysis values for some expressions in Equation 3.24.

	Fence Streamwise Linear Resistance Coefficient	Pack Thickness	Average Pressure	Pressure Difference	Specific Gas Constant	Temperature
Unit	[kg/m <sup>3</sup> s]	[mm]	[bar]	[bar]	[J/kgK]	[K]
Reference	4,262	1.372	3.77	5.5	287	298
DOE	Iteratively Calculated	Up to case	33.1	5.3	461	804

**Table 6.2: Reference and DOE conditions for calculation resistance coefficients.**

While simulations are performed, convergence problems are encountered in some cases. Small pack thickness causes oscillations in mass and momentum RMS residual values. Fluid velocity increases as a result of small clearance level between rotor surface and bristle pack and can exceed Mach 1. 18 different model are generated according to Taguchi L18 orthogonal array.

Run	Corrected Bristle Height	Minimum Pack Thickness	Porosity	Fence Streamwise Resistance Coefficient	Fence Transverse Resistance Coefficient	Pack Streamwise Resistance Coefficient	Pack Transverse Resistance Coefficient
Factor	(CBH)	(MPT)	(P)	(FSRC)	(FTRC)	(PSRC)	(PTRC)
Unit	(mm)	(mm)		(kg/m <sup>3</sup> s)	(kg/m <sup>3</sup> s)	(kg/m <sup>3</sup> s)	(kg/m <sup>3</sup> s)
1	387.5	0.829	0.1393	33668	2861780	40402	8080320
2	500	1.558	0.1180	18003	1530255	21604	4320720
3	574.4	0.677	0.1633	41542	3531070	49850	9970080
4	375.9	1.486	0.1139	18966	1612110	22759	4551840
5	481.9	0.667	0.1512	41948	3565580	50338	10067520
6	551.4	1.372	0.1265	20460	1739100	24552	4910400
7	355.9	1.184	0.1296	23721	2016285	28465	5693040
8	451.5	2.220	0.1132	12565	1068025	15078	3015600
9	513.5	0.967	0.1419	29058	2469930	34870	6973920
10	387.5	0.474	0.1633	59023	5016955	70828	14165520
11	500	1.007	0.1336	27886	2370310	33463	6692640
12	574.4	1.833	0.1165	15467	1314695	18560	3712080
13	375.9	0.549	0.1567	51224	4354040	61469	12293760
14	481.9	1.166	0.1299	24196	2056660	29035	5807040
15	551.4	2.123	0.1139	13159	1118515	15791	3158160
16	355.9	1.832	0.1165	15323	1302455	18388	3677520
17	451.5	0.822	0.1456	34496	2932160	41395	8279040
18	513.5	1.691	0.1227	16510	1403350	19812	3962400

**Table 6.3: Geometric Specifications for Design of Experiments for Ideal Gas Approach**

Run	A	B	C	D	E	F	G	H	Mass Flow	Effective Area	Effective Clearance
Factor	(RC)	(CA)	(FBH)	(BDE)	(BDIA)	(FH)	(FPT)	(BPT)			
Unit	(mil)	(deg)	(mil)	(per inch)	(mil)	(mil)	(mil)	(mil)	(kg/s)	(mm <sup>2</sup> )	(mm)
1	0	35	400	1750	4	45	30	70	0.202	40.573	0.018
2	3	35	520	2125	5	60	40	70	0.426	85.655	0.039
3	6	35	600	2500	3	75	50	70	0.755	151.934	0.069
4	6	45	400	1750	5	60	50	70	0.674	135.592	0.061
5	0	45	520	2125	3	75	30	70	0.247	49.670	0.022
6	3	45	600	2500	4	45	40	70	0.391	78.741	0.036
7	6	55	400	2125	4	75	40	70	0.703	141.559	0.064
8	0	55	520	2500	5	45	50	70	0.217	43.628	0.020
9	3	55	600	1750	3	60	30	70	0.404	81.263	0.037
10	0	35	400	2500	3	60	40	80	0.207	41.674	0.019
11	3	35	520	1750	4	75	50	80	0.445	89.605	0.040
12	6	35	600	2125	5	45	30	80	0.695	139.937	0.063
13	3	45	400	2125	3	45	50	80	0.398	80.040	0.036
14	6	45	520	2500	4	60	30	80	0.679	136.683	0.062
15	0	45	600	1750	5	75	40	80	0.311	62.581	0.028
16	3	55	400	2500	5	75	30	80	0.424	85.403	0.039
17	6	55	520	1750	3	45	40	80	0.689	138.585	0.063
18	0	55	600	2125	4	60	50	80	0.243	48.883	0.022

**Table 6.4: Design of Experiments Results for Ideal Gas Approach**

Since design parameters are determined in British units, they are given in mil and pound. Orthogonality is protected while creating design of experiments. There is a considerable difference between line-to-line, 3 mil and 6 mil cases in the aspect of leakage rate. Moreover, main effect plots for each factor is required to determine how response is changing with respect levels of design variables.

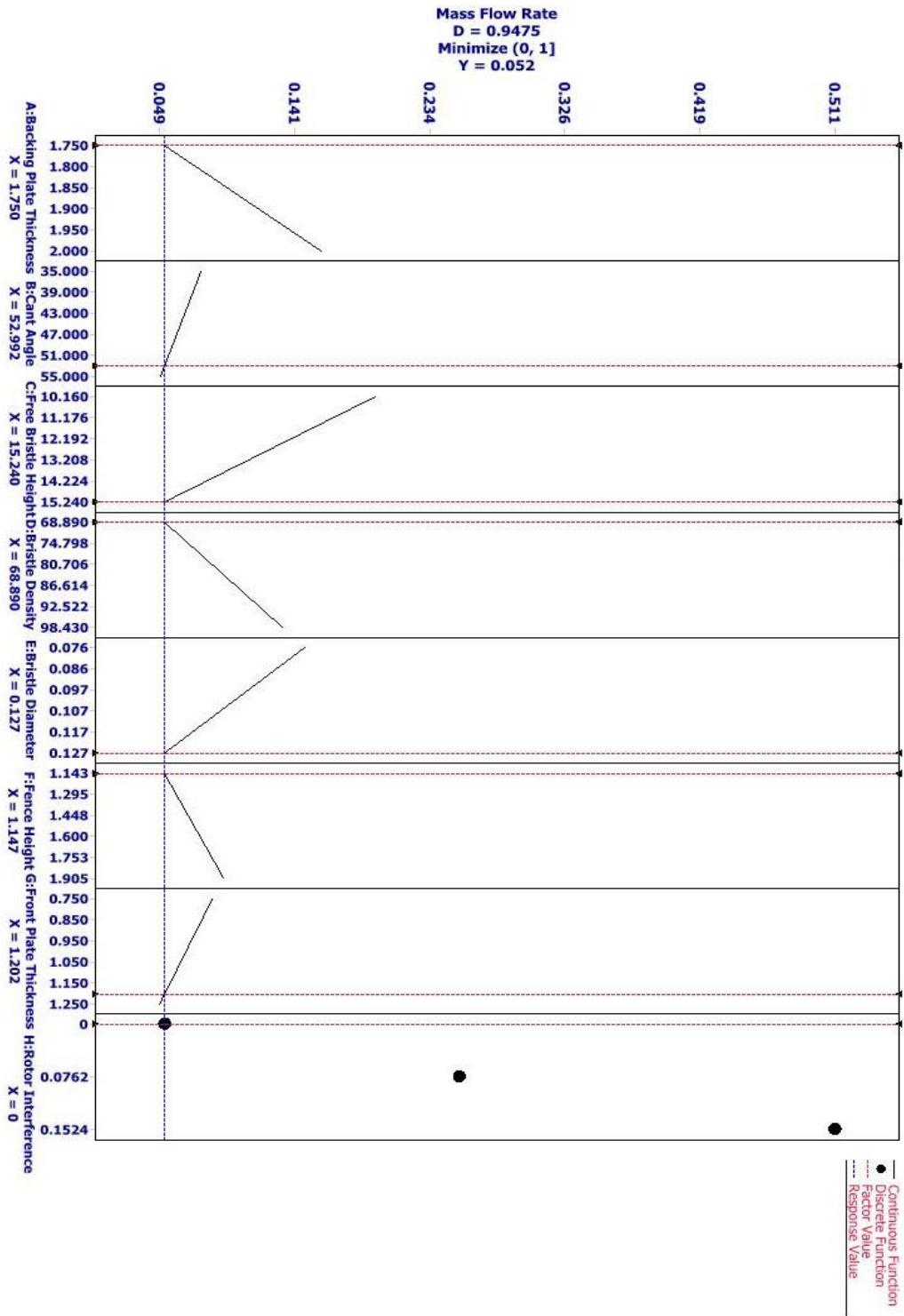


Figure 6.1: Main effect plots of factors for Ideal Gas Approach (in SI units)

## 6.4 Error Calculation for Ideal Gas Approach

T-v diagram for steam illustrated in Figure 6.2. It is shown that error rate is dependent on temperature, pressure and specific volume. Pressure and temperature levels are expressed in absolute quantities in chart. At high temperature and low specific density levels, ideal gas law for steam is not applicable. In order to determine ideal gas assumption is acceptable for this study, the exact error must be calculated. Calculation of specific volume ( $v$ ) with ideal gas law as shown in Equation 6.1.

$$R = 0.4615[kJ/kgK] \quad T = 803.15[K] \quad P_{avg} = 3310[kPa]$$
$$\text{Ideal Gas Law} \Rightarrow v = \frac{RT}{P} \quad (6.1)$$

For turbine operating conditions temperature is 530 C and pressure value is considered as average for error calculations. R is the ideal gas constant for steam.

$$v_{ideal} = \frac{0.4615[kJ/kgK] * 803.15[K]}{3310[kPa]} = 0.1120[m^3/kg] \quad (6.2)$$

Specific volume of steam is tabulated for in superheated steam tables as given in Appendix. For turbine operating conditions ( $T = 530$  [°C],  $P_{avg} = 3.31$  [MPa]), specific volume has been calculated as  $v_{actual} = 0.1105$  [m<sup>3</sup>/kg]. The difference between actual and ideal  $v$  is approximately %1.35 which is acceptable level for error.

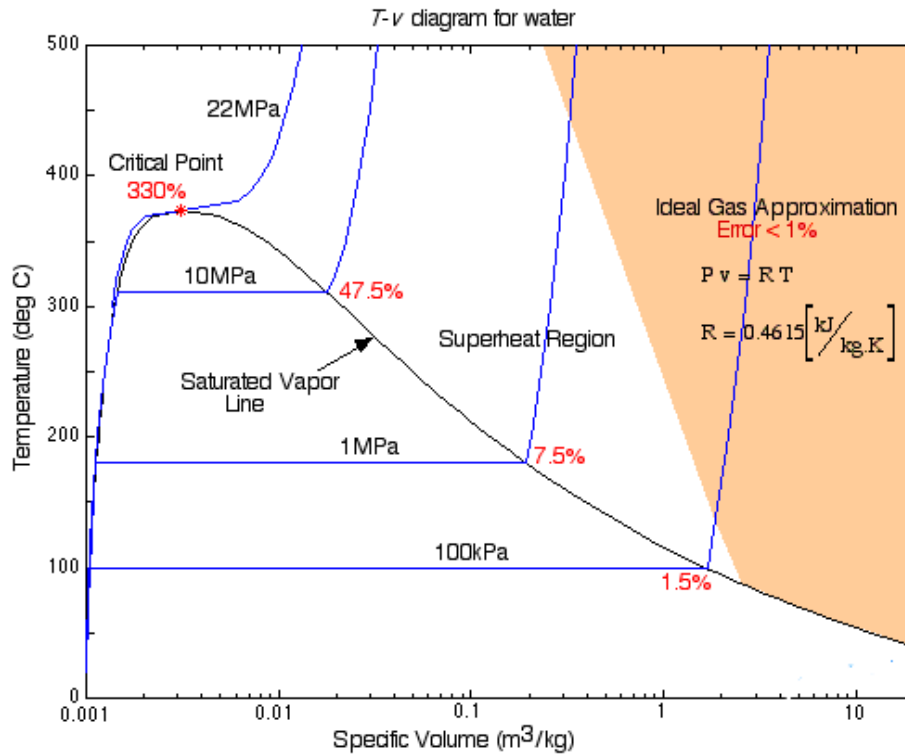


Figure 6.2: T-v Diagram for water and steam [37]

## 6.5 Design of Experiment Results for Calibration Resistance Coefficient with Pressure Difference

Once the design space is uniformly sampled using orthogonal test arrays, streamwise and transverse resistance coefficients for CFD cases have been calculated and calibrated with test data. Then, empirical relations have been derived as polynomial fits to the response. The results are plotted in Figure 6.3. As illustrated, second order polynomials fit well on the data as a trendline. First, fence height region resistance coefficients are obtained. Then, upper brush pack region resistance coefficients are easily estimated as %20 higher as per experience [36]. CFD analyses and comparative calibration work results indicated that streamwise resistance coefficients for fence height region is 85 times that of brush pack streamwise resistance coefficients. Similarly, it is approximately 200 times that of transverse resistivity coefficients in transverse direction.

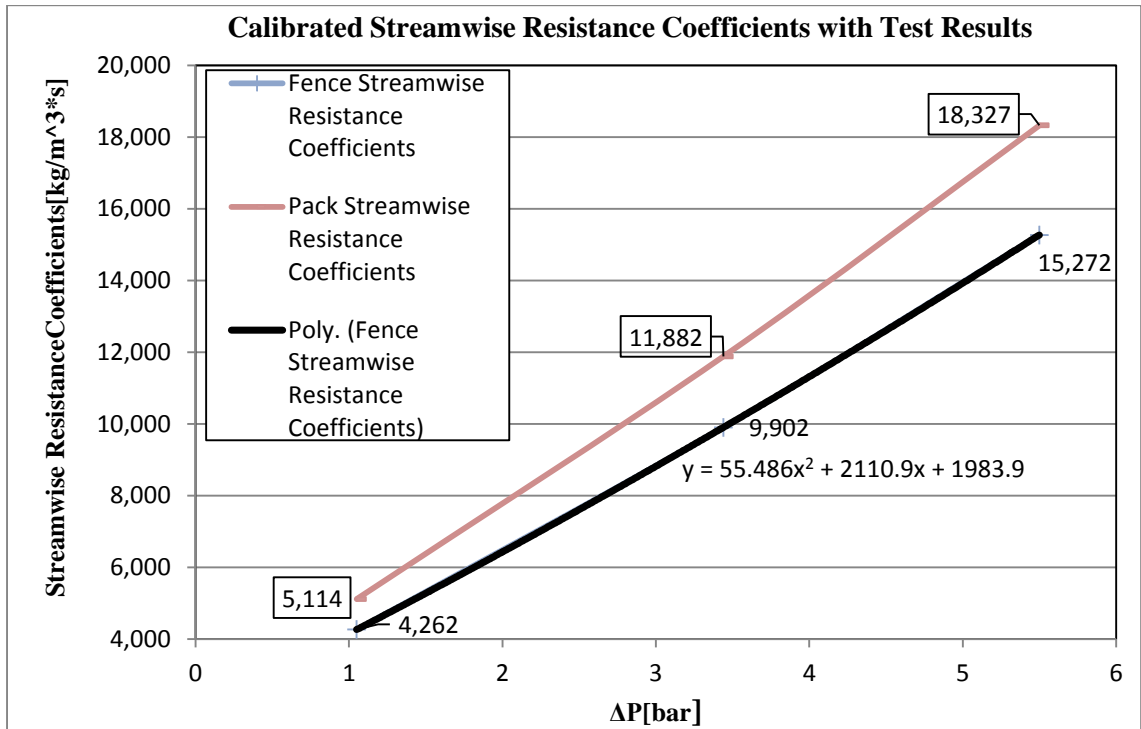


Figure 6.3: Streamwise Resistance Coefficients ( $\Delta P = 1.05, 3.44$  and  $5.5$  bar) for porous regions, line-to-line clearance configuration

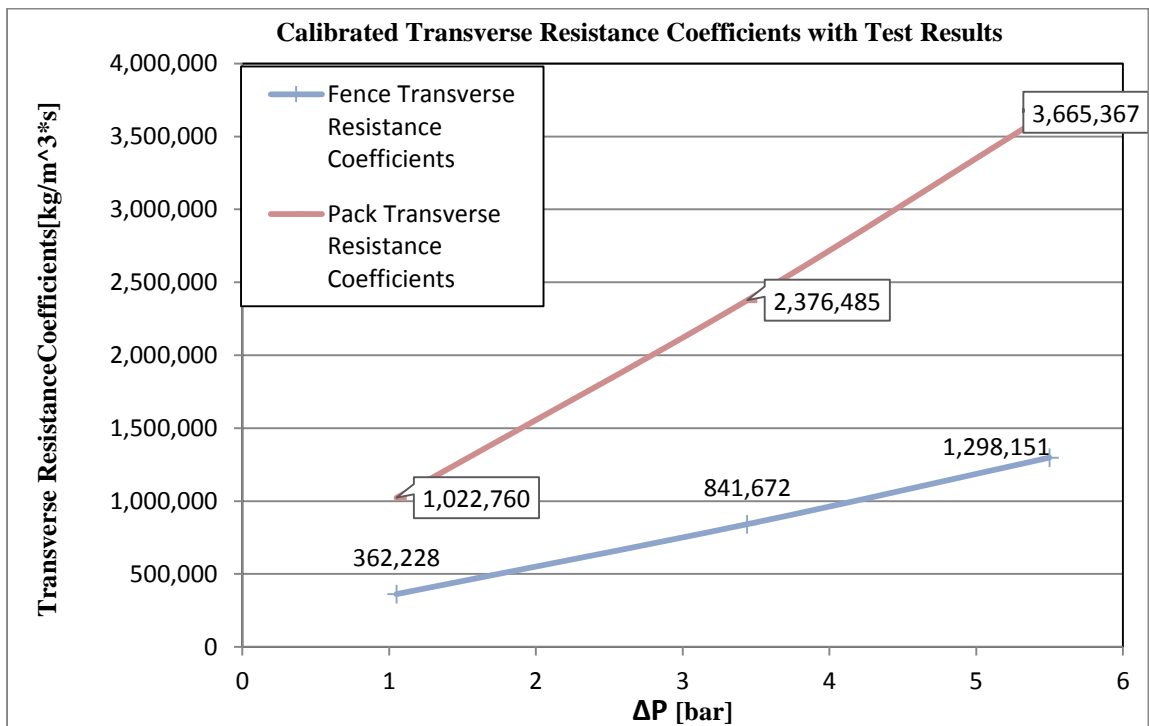


Figure 6.4: Transverse Resistance Coefficients ( $\Delta P = 1.05, 3.44$  and  $5.5$  bar) for porous regions, line-to-line clearance configuration

As an example, for  $\Delta P=5.3\text{bar}$  ( $x=5.3$ ) pressure difference condition the resistance coefficients are estimated as 14,731 [ $\text{kg/m}^3\text{s}$ ] for fence streamwise, 17,676 [ $\text{kg/m}^3\text{s}$ ] for pack streamwise, 1,252,135 [ $\text{kg/m}^3\text{s}$ ] for fence transverse, 3,535,200 [ $\text{kg/m}^3\text{s}$ ] for pack transverse.

Run	A	B	C	D	E	F	G	H	Mass Flow	Effective Area	Effective Clearance
Factor	(RC)	(CA)	(FBH)	(BDE)	(BDIA)	(FH)	(FPT)	(BPT)	(kg/s)	( $\text{mm}^2$ )	(mm)
Unit	(mil)	(deg)	(mil)	(per inch)	(mil)	(mil)	(mil)	(mil)			
1	0	35	400	1750	4	45	30	70	0.276	55.619	0.025
2	3	35	520	2125	5	60	40	70	0.447	90.002	0.041
3	6	35	600	2500	3	75	50	70	0.927	186.510	0.084
4	6	45	400	1750	5	60	50	70	0.696	140.060	0.063
5	0	45	520	2125	3	75	30	70	0.452	90.944	0.041
6	3	45	600	2500	4	45	40	70	0.408	82.207	0.037
7	6	55	400	2125	4	75	40	70	0.758	152.552	0.069
8	0	55	520	2500	5	45	50	70	0.199	40.149	0.018
9	3	55	600	1750	3	60	30	70	0.456	91.688	0.041
10	0	35	400	2500	3	60	40	80	0.383	77.143	0.035
11	3	35	520	1750	4	75	50	80	0.534	107.410	0.049
12	6	35	600	2125	5	45	30	80	0.698	140.457	0.063
13	3	45	400	2125	3	45	50	80	0.472	95.033	0.043
14	6	45	520	2500	4	60	30	80	0.728	146.490	0.066
15	0	45	600	1750	5	75	40	80	0.299	60.115	0.027
16	3	55	400	2500	5	75	30	80	0.423	85.105	0.038
17	6	55	520	1750	3	45	40	80	0.756	152.089	0.069
18	0	55	600	2125	4	60	50	80	0.253	50.994	0.023

**Table 6.5: Design of Experiments Results for Calibration Resistance Coefficients with Pressure Difference**



The results of 18 experiments are presented in Table 6.5 with specified resistance coefficients for different turbine operating conditions. L18 array allows combining evaluation of some factors at 2-levels and some at 3-levels. Backing Plate Thickness has been analyzed in two levels while other seven factor have been considered in three levels. All factors and response values have been evaluated in SI units. Pareto Chart illustrates that rotor interference, fence height, cant angle, bristle diameter have strongly impact on leakage rate whereas front plate thickness, backing plate thickness, free bristle height, and bristle density are relatively low effect on response within the defined factor ranges. The factors have been ranked based on strength. As a rule of thumb, approximately half of the factors are selected as strong factors rests are defined as weak.

Figure 6.5 illustrates trends of factors for each level, represents optimal design. Leakage rate can be decreased by reducing, fence height and rotor interference level; increasing cant angle, bristle diameter.

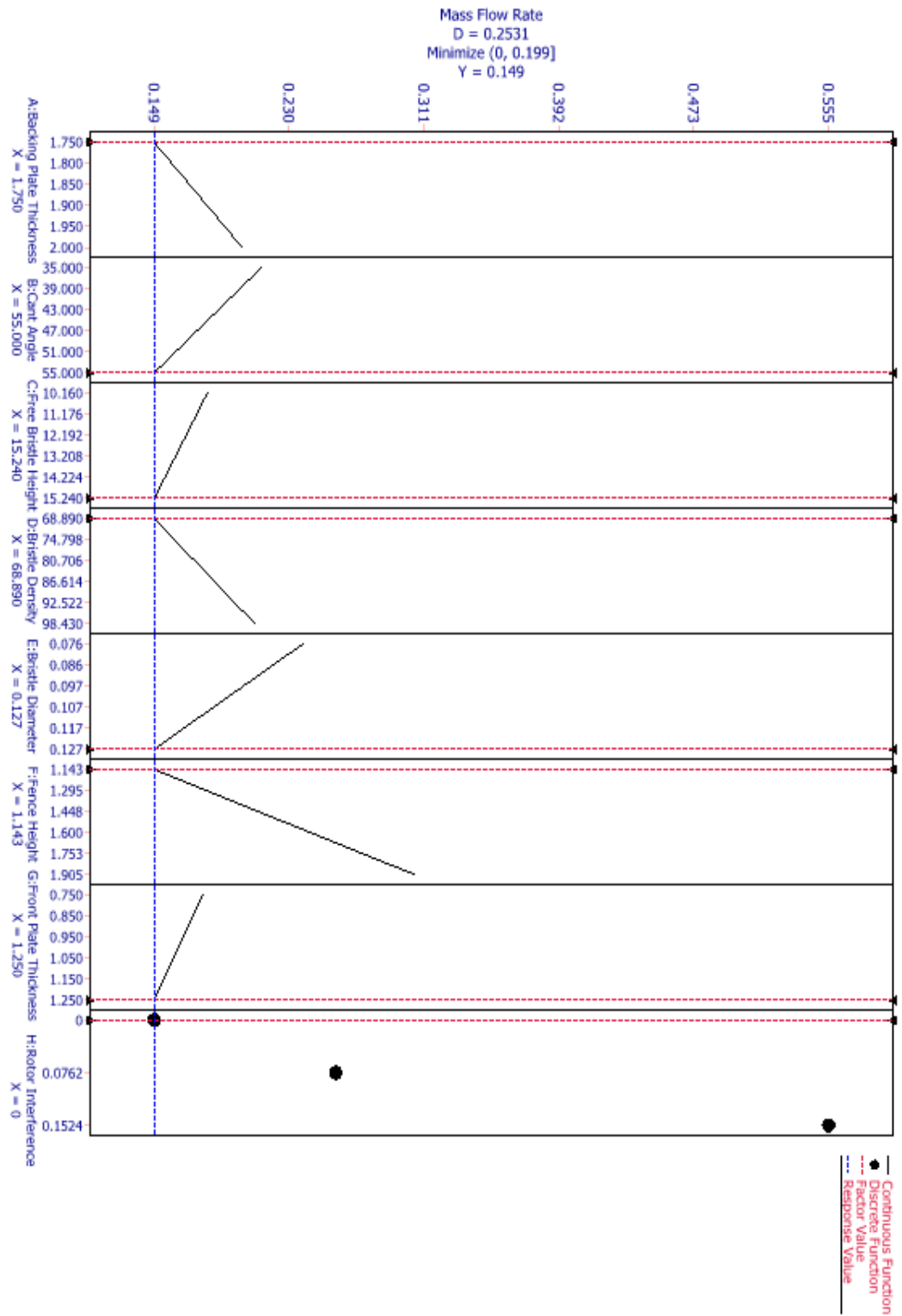
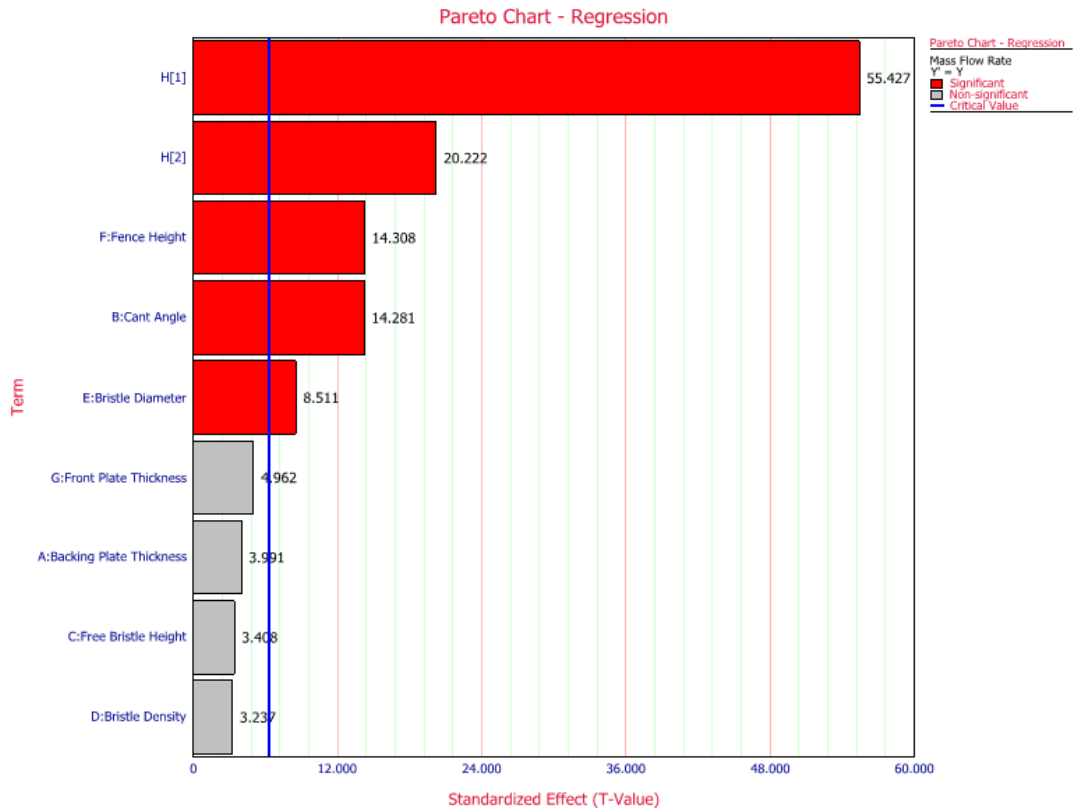


Figure 6.5: Main effect plots of factors for Pressure Difference Approach



**Figure 6.6: Pareto Chart for leakage rate**

The results indicate that rotor interference is the most important parameter which have impact on leakage performance. This is attributed to the fact that leakage area between rotor and backing plate as well as the fact that brush porosity is altered as rotor pushes bristles. Fence height is another crucial factor as it determines allowed leakage area in fence region. Cant angle directs fluid to move tangentially which contributes flow velocity in third direction. Bristle diameter has major impact on brush porosity which also show in results. Once the bristle diameter is fixed, bristle density only effects the brush pack thickness. It has significant effect on overall leakage, but not on resistivity coefficients which are dominated by bristle diameter. Free bristle height, front and backing plate thickness have limited effect on flow resistivity coefficients as seen Figure 6.6. Therefore, they are defined as weak factors.

Leakage Rate Equation Estimated (fit) Values for Coefficients				
		For Coded Factor Values		For Actual Factor Values
Index of Coefficient	Coefficient Term	Coefficient Value		Coefficient Value
0	Constant	+0.5097		-6.2594
1	BPT	+0.0103		+3.7417
2	CA	-0.0372		+0.0038
3	FBH	-0.0080		+0.1716
4	BDE	-0.0118		+0.0210
5	BDIA	-0.0277		+6.1524
6	FH	+0.0494		+1.2767
7	FPT	-0.0147		-0.0587
8	RC[1]	-0.1718		-0.1718
9	RC[2]	-0.0624		-0.0624
10	BPT * CA	-0.0050		-0.0040
11	BPT * FBH	-0.0296		-0.0932
12	BPT * BDE	-0.0266		-0.0144
13	BPT * BDIA	-0.0049		-1.5525
14	BPT * FH	-0.0291		-0.6117
15	FBH * BDE	+0.0155		+0.0004
16	FBH * BDIA	-0.0220		-0.3410

**Table 6.6: Fit Values for Coefficients of Leakage Rate for both Coded and Actual Values**

## 6.6 Minimum Leakage Solution

Table 6.7 illustrates optimization settings which allows to specify how calculations are performed. Design Runs specifies the number of runs in the design which will be checked for optimal solutions. Random Runs specifies the number of random start points that will be analyzed. Simplex Algorithm Epsilon is the convergence criterion that controls how long program try to find optimal solutions. Fractions identifies the width of the range from each start point that will be checked for optimal solutions. Seed allows the user to specify a beginning point for the random number generation used in the optimization process, providing repeatability of results.

<b>Optimization Settings</b>	
<b>Response Settings</b>	
Goal	Minimize
Target Value	0
Upper Limit	0.7550
<b>Algorithm Settings</b>	
Design Runs	10
Random Runs	30
Simplex Algorithm Epsilon	1E-06
Fractions	1, 0.8, 0.5, 0.2, 0.05
Seed	1

**Table 6.7: Response and Algorithm Settings**

For a given set of factors, a linear response trend is assumed for two-level evaluations. For 3-level evaluations nonlinear response behavior can be captured where midpoint can be selected as optimal level. Based on the results of 18 simulation runs, an optimum design combination has been estimated using Taguchi techniques. Table 6.8 reveals optimal levels of design variables for a minimum leakage case for the selected design space, and presents the corresponding response. Optimized designs have less mass flow rates than all of the 18 cases that are performed in design of experiments.

An optimum design combination has been estimated using Taguchi techniques. Optimal solution has been reached in the range of determined factor levels. Due to manufacturing limitations, optimum solution is not searched for wider range of design parameters. For example, designing a seal with a fence height as less than 15.24 [mm] may decrease leakage rate, however, typical rotor excursions do not allow such a tight shaft clearance. Leakage rate of optimal solution is less than leakage rate of all 18 designs as shown in Tables 6.4 and 6.5. The results indicate that for high flow resistivity and minimum leakage flow. In the literature, reducing fence height and rotor-bristle pack clearance decreases leakage rate which is consistent with optimized results [5, 38]. Although, effect of front and backing plate geometry on brush seal pressure and flow fields have been studied [39, 40], there is lack of study that explains the relationship between thickness of plates and leakage performance.

<b>Optimal Solution</b>									
Factor	Rotor Clearance	Cant Angle	Free Bristle Height	Bristle Density	Bristle Diameter	Fence Height	Front Plate Thickness	Backing Plate Thickness	Leakage Rate

Unit	[mm]	[deg]	[mm]	[per mm]	[mm]	[mm]	[mm]	[mm]	[kg/s]
Ideal Gas	0	53	15.24	68.89	0.127	1.1475	1.2025	1.75	<b>0.1995</b>
Pressure Difference	0	55	15.24	68.89	0.127	1.143	1.25	1.75	<b>0.1957</b>

**Table 6.8: Optimal Solution for Calibration Resistance Coefficients with Ideal Gas and Pressure Difference Approach**

## 7 CONCLUSION

Brush seals have been integrated in turbine applications with harsh pressure and temperature conditions. Leakage rate and effective clearance are main issues that determine seal overall performance. Rotor interference, fence height, cant angle and bristle diameter have strongly influence on brush porosity and leakage performance due to the fact that they affect fluid velocity profile and flow behavior. Complex interactions between brush seal, rotor and plates makes it complicated to estimate leakage rate, velocity profile and pressure distribution over the entire brush seal region. Among different approaches to model brush seal leakage flow, porous medium modeling of bristle pack provides the most insight to help designers. However, flow resistance/porosity coefficients for these porous media CFD models have to be calibrated with experimental seal leakage test data for each design. To meet this need, a design of experiments test matrix has been defined with some typical ranges of main seal design parameters. The selected design space has been uniformly sampled using orthogonal arrays. The results have been evaluated to determine strong and weak factors affecting flow resistivity. Polynomial fits and empirical relations have been derived using the design factors that strongly affect brush flow resistivity. It is expected that these empirical relations may guide designers when they estimate performance of different brush seal designs. Moreover, and optimization of design parameters for a minimum porosity brush seal design has been completed and presented. Differently, this study provides correlation between air environment test data and steam environment CFD models.

Apart from the main contribution presented above, the following detail tasks have been achieved during the course of this study:

- **Analytical Studies and Correlation with Tests**
  - Brush seal permeability coefficients have been expressed in Darcian porous model.
  - Porosity and minimum pack thickness calculation have been presented.
  - The estimation of resistance coefficients has been performed for new designs by involving reference resistance coefficients, pack thickness, average pressure, pressure difference, temperature and specific gas constant.

- Effective clearance calculations have been expressed for both choked and unchoked flow. It has been applied to compare brush seal leakage performance for different cases and geometries.
  - The correction of free bristle height has been performed in a MATLAB code which is required for accurate representation of the seal inner and outer diameter in two-dimensional plane.
- **Rotary Test Rig Design**
    - Test seals have been chosen and procured.
    - Custom tests have been planned and performed at 3600 rpm.
    - Six different brush seals have been tested to measure leakage rate and effective clearance values have been calculated.
    - Rotor-stator dynamic simulations have been conducted with test results for identifying resistance coefficients of brush seals.
- **Brush Seal CFD Analyses and Correlation with Tests**
    - Porous medium brush modeling approach has been successfully applied in CFD models.
    - The presented CFD models have successfully simulated the tested brush seals.
    - Resistance coefficients have been iteratively calibrated.
    - The model estimations have been successfully matched with experimental and analytical data.
- **Design Optimization Based on CFD**
    - Design optimization study have been performed to systematically investigate effect of rotor interference, cant angle, free bristle height, bristle density, bristle diameter, fence height, front plate thickness and backing plate thickness.
    - Porosity, pack thickness and resistance coefficient calculators have been prepared to find correct values quickly which may be used for various other design.
    - Turbine operating conditions have been applied in CFD models as boundary conditions. More than 40 cases have been successfully simulated and converged with acceptable residual targets.



- L18 Taguchi arrays has been applied to uniformly sample a design space and to reach an optimum solution. It has been set to analyze seven factors in three-levels and one factor in two-levels.
- Pareto chart and main effect plots have been generated to illustrate how response varies with respect to each level of factors.
- Results show that rotor interference, fence height, cant angle and bristle diameter have strongly impact on porosity and leakage performance of brush seal for the specified operating conditions.

Correlation may be extended between air and steam test data as next study to validate formulations. Moreover, geometry may also be included in the correlation comprehensively so there is no need to perform tests for each brush seal design.

## 8 REFERENCES

- [1] Pastrana, M.R., Wolfe, C.E., Turnquist, N.A. and Burnett, M.E., “Improved Steam Turbine Leakage Control with a Brush Seal Design”, Proceedings of the 30<sup>th</sup> Turbomachinery Symposium, 33-38.
- [2] Turnquist, N., Chupp, R., Baily, F., Burnett, M., Rivas, F., Bowsher, A. and Crudginton, P., “Brush Seals for Improved Steam Turbine Performance”, NASA Seals Workshop, NASA/CP-2006-214383/VOL1, 107-127.
- [3] Childs, P.R.N, “Labyrinth Seal Flow”, ESDU 09004, (2009).
- [4] <http://www.haynesintl.com/literature.htm>
- [5] Aksit, M. F., “A Computational Study of Brush Seal Contact Loads with Friction”, Thesis Project for Doctor of Philosophy, Rensselaer Polytechnic Institute, Troy, New York, (1998).
- [6] Ferguson, J.G., “Brushes as High Performance Gas Turbine Seals”, ASME Gas Turbine and Aeroengine Congress Paper ASME 88-GT-182, (1988).
- [7] ‘Ferranti Fluid Packing’, Patent No. 885,032, (1908).
- [8] Flower, R., ‘Brush Seal Development System’, AIAA/ASME/SAE/ ASEE/ 26<sup>th</sup> Joint Propulsion Conference, AIAA Paper 90-2143.
- [9] Mahler, F. and Boyes, E., ‘The Application of Brush Seals in Large Commercial Jet Engines’, AIAA/ASME/SAE/ASEE 31<sup>st</sup> Joint Propulsion Conference, San Diego, California (1995).
- [10] Gorelov, G.M., Reznik, V.E. and Tsbizov, V.I., ‘Experimental Study of Brush Seal Flow Characteristics and Comparison with a Labyrinth Seal’ Izvestiya VUZ. Aviatsionnaya Takhnika, 31, pp 43-46, (1988).
- [11] Dinc, S., Bagepalli, B., Cromer, R.H., Maynard, J., Calabrese, S. and Aksit, M.F., ‘High Temperature Vibratory Brush Seals for Gas Turbine Applications’ ,

- AIAA/SAE/ASME/ASEE 30<sup>th</sup> Joint Propulsion Conference Paper AIAA 94-2704, (1994).
- [12] Wolfe, C.E., Chiu, R.P., Cromer, R.H., Marks, P.T., Stuck, A.E., Turnquist, N.A., Reluczo, G and Dinc, O.S., 'Brush Seals in Industrial Gas Turbines' , AIAA/ASME/SAE/ASEE 33<sup>rd</sup> Joint Propulsion Conference, AIAA Paper No. 97-2730, Seattle, Washington.
- [13] Holle, G.F., and Khrishnan, M.R., 'Gas Turbine Engine Brush Seal Applications', AIAA/SAE/ASME/ASEE 26<sup>th</sup> Joint Propulsion Conference Paper AIAA 90-2142, (1990).
- [14] Mayhew, E.R., Bill, R.C., Voorhees, W.J. and O'Donnell, J., 'Military Engine Seal Development: Potential for Dual Use', AIAA/SAE/ASME/ASEE 30<sup>th</sup> Joint Propulsion Conference Paper AIAA 94-2699, (1994).
- [15] Owen, A.K., Jones, T.V., Guo, S.M. and Hogg, S., 'An Experimental and Theoretical Study of Brush Seal and Shaft Thermal Interaction', ASME paper no. GT-2003-38276 (2003).
- [16] Chew, J. W., and Guardino, C., 'Simulation Flow and Heat Transfer in the Tip Region of a Brush Seal', Int. J. Heat Fluid Flow, 25, No. 4, pp 649-658, (2004).
- [17] Demiroglu, M., 'An Investigation of Tip Force and Heat Generation Charactersitics of Brush Seals', Ph.D. Thesis, Rensselaer Polytechnic Institute , Troy, NY, USA, (2004).
- [18] Dogu, Y., and Aksit, M., 'Brush Seal Temperature Distribution Analysis', ASME J. Eng. For Gas Turbines and Power, 128, pp. 599-609, (2006).
- [19] Braun, M. and Canacci, V., 'Flow visualization and Motion Analysis for a Series of Four Sequential Brush Seals' AIAA/SAE/ASME/ASEE 26<sup>th</sup> Joint Propulsion Conference Paper AIAA 90-2482, (1990).
- [20] Braun, M., Hendricks, R.C. and Yang, Y., 'Effects of Brush Seal Morphology on Leakage and Pressure Drops' AIAA/SAE/ASME/ASEE 27<sup>th</sup> Joint Propulsion Conference Paper AIAA 91-2106, (1991).

- [21] Braun, M., Hendricks, R.C. and Canacci, V., 'Flow Visualization in a Simulated Brush Seal' ASME Gas Turbine and Aeroengine Congress Paper ASME 90-GT-217 (1990).
- [22] Carlile, J.A., Hendricks, R.C. and Yoder, D.A., 'Brush Seal Leakage Performance with Gaseous Working Fluids at Static and Low Rotor Speed Conditions' ASME Trans. J. Eng. For Gas Turbines and Power, 115, pp 397-403, (1993).
- [23] Braun, M.J., Canacci, V.A., and Hendricks, R.C., 'Flow Visualization and Quantitative Velocity and Pressure Measurements in Simulated Single and Double Brush Seals' Trib., Trans., 34, pp 70-80, (1991).
- [24] Braun, M.J. and Kudriatsev, V.V., 'A numerical Simulation of a Brush Seal Section and Some Experimental Results' ASME Gas Turbine and Aeroengine Congress Paper ASME 93-GT-398, (1993).
- [25] Kudriatsev, V.V. and Braun, M.J., 'A Reynolds Number Parametric Numerical Investigation of Flow Structures and Pressure Distribution in a System of Cylinder Arrays' Proc. Of ASME Int. Fluid Eng. Conf., FED-Vol. 149, Washington, D.C., pp 83-93, (1993).
- [26] Mullen, R., Braun, M.J. and Hendricks, R.C., 'Numerical Modelling of Flows in Simulated Brush Seal Configurations' AIAA/SAE/ASME/ASEE 26<sup>th</sup> Joint Propulsion Conference Paper AIAA 90-2141, (1990).
- [27] Sharatchandra, M.C. and Rhode, D.L., 'Computed Effects of Rotor-Induced Swirl on Brush Seal Performance - Part 1: Leakage Analysis' ASME Trans. J. Trib., 118, pp- 912-919, (1996).
- [28] Hendricks, R.C., Braun, M.J., Canacci, V.A. and Mullen, R., 'Brush Seals in Vehicle Tribology' Proc. of the 13<sup>th</sup> Leeds-Lyon Symp. On Tribology, Paper E-5712, Leeds, England, (1990).
- [29] Hendricks, R.C., Schlumberger, S., Braun, M.J., Choy, F. and Mullen, R.L., 'A Bulk Flow Model of Brush Seal System' ASME Gas Turbine and Aeroengine Congress Paper ASME 91-GT-325, (1991).

- [30] Braun, M.J., Hendricks, R.C. and Canacci, V.A., ‘Non-Intrusive and Quantitive Flow Characterization and Bulk Flow Model for Brush Seals’ Proc. of the Japan Int. Trib. Conf. , 2, Nagoya, Japan, pp 1611-1616, (1990).
- [31] Bayley, F.J. and Long, C.A., ‘A Combined Experimental and Theoretical Study of Flow and Pressure Distributions in a Brush Seal’ ASME Trans. J. Eng. for Gas Turbines and Power, 115, pp-404-410, (1993).
- [32] Chew, J.W., Lapworth, B.L. and Millener, P.J., ‘Mathematical Modeling of Brush Seals’ Int. J, Heat and Fluid Flow, 16, pp 493-500, (1995).
- [33] Chew, J.W. and Hogg, S.I., ‘Porosity Modeling of Brush Seals’ ASME Trans. J. Trib., 119, pp 769-775, (1997).
- [34] Turner, M.T., Chew, J.W. and Long, C.A., ‘Experimental Investigation and Mathematical Modelling of Clearance Brush Seals’ ASME Gas Turbine and Aeroengine Congress Paper ASME 97-GT-282, (1997).
- [35] Duran, E. T., “Stiffness and Friction Characterization of Brush Seals”, Thesis Project for Doctor of Philosophy, Sabanci University, Istanbul, (2013).
- [36] Dogu, Y., “Investigation of Brush Seal Flow Characteristics Using Bulk Porous Medium Approach,” ASME Journal of Engineering for Gas Turbines and Power, Vol. 127, No. 1, pp. 136-144, (2005).
- [37] [http://www.ohio.edu/mechanical/thermo/Intro/Chapt.1\\_6/Chapter2b.html](http://www.ohio.edu/mechanical/thermo/Intro/Chapt.1_6/Chapter2b.html)
- [38] Dogu, Y., and Aksit, M., Demiroglu, M., Dinc, O.S., ‘Evaluation of Flow Behaviour for Clearance Brush Seals’, ASME J. Eng. For Gas Turbines and Power, 128, pp. 599-609, (2008).
- [39] Dogu, Y., and Aksit, M., ‘Effects of Geometry on Brush Seal Pressure and Flow Fields- Part 1: Front Plate Configurations’, ASME J. of Turbomachinery, 128, pp. 367-378, (2006).
- [40] Dogu, Y., and Aksit, M., ‘Effects of Geometry on Brush Seal Pressure and Flow Fields- Part 2: Backing Plate Configurations’, ASME J. of Turbomachinery, 128, pp. 379-389, (2006).

## APPENDIX

### Superheated Vapor Properties for Steam – (1.6 MPa – 3.5 MPa)

P=1.80 MPa (207.1°C)				P=2.00 MPa (212.4°C)				P=1.60 MPa (201.4°C)				
volume	energy	enthalpy	entropy	volume	energy	enthalpy	entropy	Temp	volume	energy	enthalpy	entropy
v(m <sup>3</sup> /kg)	u(kJ/kg)	h(kJ/kg)	s(kJ/kg.K)	v(m <sup>3</sup> /kg)	u(kJ/kg)	h(kJ/kg)	s(kJ/kg.K)	°C	v(m <sup>3</sup> /kg)	u(kJ/kg)	h(kJ/kg)	s(kJ/kg.K)
0.1104	2597.2	2795.9	6.378	0.0996	2599.1	2798.3	6.339	Sat	0.1237	2594.8	2792.8	6.420
0.1168	2637.0	2847.2	6.482	0.1038	2628.5	2836.1	6.416	225	0.1329	2645.1	2857.8	6.554
0.1250	2686.7	2911.7	6.609	0.1115	2680.2	2903.2	6.548	250	0.1419	2692.9	2919.9	6.675
0.1403	2777.4	3029.9	6.825	0.1255	2773.2	3024.2	6.768	300	0.1587	2781.6	3035.4	6.886
0.1546	2863.6	3141.8	7.012	0.1386	2860.5	3137.7	6.958	350	0.1746	2866.6	3146.0	7.071
0.1685	2948.3	3251.6	7.181	0.1512	2945.9	3248.3	7.129	400	0.1901	2950.7	3254.9	7.239
0.1821	3033.1	3360.9	7.338	0.1635	3031.1	3358.2	7.287	450	0.2053	3035.0	3363.5	7.395
0.1955	3118.5	3470.4	7.485	0.1757	3116.9	3468.2	7.434	500	0.2203	3120.1	3472.6	7.541
0.2220	3292.7	3692.3	7.754	0.1996	3291.5	3690.7	7.704	600	0.2500	3293.9	3693.9	7.810
0.2482	3472.6	3919.4	8.000	0.2233	3471.6	3918.2	7.951	700	0.2794	3473.5	3920.5	8.056
0.2743	3658.8	4152.4	8.228	0.2467	3658.0	4151.5	8.179	800	0.3087	3659.5	4153.3	8.283
0.3002	3851.5	4391.9	8.442	0.2701	3850.9	4391.1	8.393	900	0.3378	3852.1	4392.6	8.497
0.3261	4050.7	4637.6	8.643	0.2934	4050.2	4637.0	8.594	1000	0.3669	4051.2	4638.2	8.697

P=3.0 MPa (233.9°C)				P=3.5 MPa (242.6°C)				P=2.5 MPa (224.0°C)				
volume	energy	enthalpy	entropy	volume	energy	enthalpy	entropy	Temp	volume	energy	enthalpy	entropy
v(m <sup>3</sup> /kg)	u(kJ/kg)	h(kJ/kg)	s(kJ/kg.K)	v(m <sup>3</sup> /kg)	u(kJ/kg)	h(kJ/kg)	s(kJ/kg.K)	°C	v(m <sup>3</sup> /kg)	u(kJ/kg)	h(kJ/kg)	s(kJ/kg.K)
0.0667	2603.2	2803.2	6.186	0.0571	2602.9	2802.6	6.124	Sat	0.0800	2602.1	2801.9	6.256
0.0706	2644.7	2856.5	6.289	0.0588	2624.0	2829.7	6.176	250	0.0871	2663.3	2880.9	6.411
0.0812	2750.8	2994.3	6.541	0.0685	2738.8	2978.4	6.448	300	0.0989	2762.2	3009.6	6.646
0.0906	2844.4	3116.1	6.745	0.0768	2836.0	3104.8	6.660	350	0.1098	2852.5	3127.0	6.842
0.0994	2933.5	3231.7	6.923	0.0846	2927.2	3223.2	6.843	400	0.1201	2939.8	3240.1	7.017
0.1079	3021.2	3344.8	7.086	0.0920	3016.1	3338.0	7.007	450	0.1302	3026.2	3351.6	7.177
0.1162	3108.6	3457.2	7.236	0.0992	3104.5	3451.6	7.159	500	0.1400	3112.8	3462.7	7.325
0.1325	3285.5	3682.8	7.510	0.1133	3282.5	3678.9	7.436	600	0.1593	3288.5	3686.8	7.598
0.1484	3467.0	3912.2	7.759	0.1270	3464.7	3909.3	7.685	700	0.1784	3469.3	3915.2	7.846
0.1642	3654.3	4146.9	7.989	0.1406	3652.5	4144.6	7.916	800	0.1972	3656.2	4149.2	8.074
0.1799	3847.9	4387.5	8.203	0.1541	3846.4	4385.7	8.130	900	0.2160	3849.4	4389.3	8.288
0.1955	4047.7	4634.1	8.405	0.1675	4046.4	4632.7	8.332	1000	0.2347	4048.9	4635.6	8.490